AFRL-AFOSR-UK-TR-2011-0037

NOVEL ANTENNAS BASED UPON EXTRAORDINARY TRANSMISSION METAMATERIAL LENSES

MARIO SOROLLA

UNIVERSIDAD PUBLICA DE NAVARRA
ELECTRICAL AND ELECTRONIC ENGINEERING
EDIFICIO LOS TEJOS
PAMPLONA, SPAIN 31006

EOARD GRANT 10-3078

August 2011

Final Report for 03 August 2010 to 03 August 2011

Air Force Research Laboratory
Air Force Office of Scientific Research
European Office of Aerospace Research and Development
Unit 4515 Box 14, APO AE 09421

REPORT DOCUMENTATION PAGE

Form Approved OMB No. 0704-0188

1. REPORT DATE *(DD-MM-YYYY)*	2. REPORT TYPE	3. DATES COVERED *(From – To)*
04-08-2011	Final Report	03 August 2010 - 03 August 2011

4. TITLE AND SUBTITLE

NOVEL ANTENNAS BASED UPON EXTRAORDINARY TRANSMISSION METAMATERIAL LENSES

5a. CONTRACT NUMBER

FA8655-10-1-3078

5b. GRANT NUMBER

Grant 10-3078

5c. PROGRAM ELEMENT NUMBER

6. AUTHOR(S)

Professor Mario Sorolla

5d. PROJECT NUMBER

5d. TASK NUMBER

5e. WORK UNIT NUMBER

7. PERFORMING ORGANIZATION NAME(S) AND ADDRESS(ES)

UNIVERSIDAD PUBLICA DE NAVARRA
ELETRICAL AND ELECTRONIC ENGINEERING
EDIFICIO LOS TEJOS
PAMPLONA, SPAIN 31006

8. PERFORMING ORGANIZATION REPORT NUMBER

N/A

9. SPONSORING/MONITORING AGENCY NAME(S) AND ADDRESS(ES)

EOARD
Unit 4515 BOX 14
APO AE 09421

10. SPONSOR/MONITOR'S ACRONYM(S)

AFRL/AFOSR/RSW (EOARD)

11. SPONSOR/MONITOR'S REPORT NUMBER(S)

AFRL-AFOSR-UK-TR-2011-0037

12. DISTRIBUTION/AVAILABILITY STATEMENT

Approved for public release; distribution is unlimited. (approval given by local Public Affairs Office)

13. SUPPLEMENTARY NOTES

14. ABSTRACT

A deep analysis of bi- and plano-concave lens antennas made of stacked doubly period subwavelength hole arrays in terms of focus and angular power distribution is presented in this report. The key difference between these Left-Handed Extraordinary Transmission lenses (LHET-lenses) and the classical metallic lenses is based on the fact that contrary to the latter ones, LHET-lenses work in the cut-off region of the circular waveguide formed by consecutive stacked holes. This leads to a negative index of refraction, whereas metallic lenses exhibit a positive but less than one index of refraction. Another activity done during this project is related with directivity enhancement by a short-focal-length plano-concave lens engineered by stacked subwavelength hole arrays (fishnet-like stack) with an effective negative index of refraction close to zero, $n \rightarrow 0$, that arises from ε and μ near-zero extreme values.
The possible applications of these novel lenses in antenna engineering have been opened.

15. SUBJECT TERMS

EOARD, metamaterials

16. SECURITY CLASSIFICATION OF:			17. LIMITATION OF ABSTRACT	18, NUMBER OF PAGES	19a. NAME OF RESPONSIBLE PERSON
a. REPORT	b. ABSTRACT	c. THIS PAGE			SCOTT DUDLEY, Lt Col, USAF
UNCLAS	UNCLAS	UNCLAS	SAR	42	19b. TELEPHONE NUMBER *(Include area code)* +44 (0)1895 616162

EUROPEAN OFFICE OF AEROSPACE RESEARCH AND DEVELOPMENT (EOARD), US AIR FORCE RESEARCH LABORATORY

REPORT ON GRANT FA 8655-10-1-3078, "Novel Antennas Based Upon Extraordinary Transmission Metamaterial Lenses"

Done in Pamplona, Navarra, Spain on July 18th 2011.

Prof. Mario Sorolla Ayza

Team: Prof. Francisco Falcone Lanas, Dr. Miguel Beruete Díaz, and Dr. Miguel Navarro Cía.

MILLIMETER AND TERAHERTZ WAVES LABORATORY
ELECTRICAL AND ELECTRONIC ENGINEERING DEPARTMENT
PUBLIC UNIVERSITY OF NAVARRE
E-31006 PAMPLONA, NAVARRE, SPAIN
Phone: +34948169324
Telefax: +34948169720
e-mail: mario@unavarra.es
http://www.csm.unavarra.es/

TABLE OF CONTENTS

LIST OF FIGURES

comparison purpose and excited by a dipole. (c) Idem for LHET-lens antenna with dimensions of fabricated prototype.

Fig. 10. Sketch of the experimental set-up for the angular pattern measurement of the set open-rectangular-waveguide-LHET-lens. (Insights) Pictures of the real set-up.

Fig. 11. Co-polar (top) and cross-polar (middle) measurements of the angular power distribution as a function of frequency for E-plane (left column) and H-plane (right column) under open-ended waveguide illumination. (Bottom) Cut-frequency at 54.2 GHz of preceding graphs. Excitation and reception was done using open waveguide and corrugated horn antenna, respectively.

Fig. 12. Co-polar (top) and cross-polar (bottom) measurements of the angular power distribution as a function of frequency for H-plane when the feed is a resonant slot and receptor is a horn antenna.

Fig. 13. Reflection coefficient of the LHET-lens antenna when it is illuminated by means of a corrugated horn antenna placed at the lens focus.

LIST OF TABLES

SUMMARY

A deep analysis of bi- and plano-concave lens antennas made of stacked doubly period subwavelength hole arrays in terms of focus and angular power distribution is presented in this report. The key difference between these Left-Handed Extraordinary Transmission lenses (LHET-lenses) and the classical metallic lenses is based on the fact that contrary to the latter ones, LHET-lenses work in the cut-off region of the circular waveguide formed by consecutive stacked holes. This leads to a negative index of refraction, whereas metallic lenses exhibit a positive but less than one index of refraction.

Another activity done during this project is related with directivity enhancement by a short-focal-length plano-concave lens engineered by stacked subwavelength hole arrays (fishnet-like stack) with an effective negative index of refraction close to zero, $n \rightarrow 0$, that arises from ε and μ near-zero extreme values.

The possible applications of these novel lenses in antenna engineering have been opened.

INTRODUCTION

It is well-known that artificial dielectric materials were used to alleviate experimental difficulties of performing measurements of electromagnetic waves propagating in plasmas in the 60's of the last century [1]. However, artificial dielectric materials trace back to the 40's, when they were initially used as beamformers for antenna applications. Pioneering work in metallic lens founded on parallel metallic plates was done by Kock [2,3] The combination of line lengths - in the case of TE-lens as a result of a different phase velocity relative to free space, whereas in the case of TEM-lens due to an increment of the physical length - and array geometries acts as a phase transformer, converting the spherical wave emitted by the feed into a plane wave or in the other way round, focusing the incident plane wave into a spot. Outstanding in the TE-lens is that concave and convex change its role compared with common dielectric lenses because of the positive but less than one index of refraction, $0 < n < 1$, of the first propagation mode of this parallel plates waveguide.

Similar to common dielectric lenses, the artificial metallic TE-lens has a tradeoff between matching and thickness. When the index of refraction is closer to 1, the reflection is lower but the lens needs to be thicker to achieve focusing. On the other hand, the closer the n is to 0 the thinner the lens will be, but also the greater the mismatch. These properties arise as a result of the non variability of the magnetic permeability μ, which is considered $\mu = 1$.

TE-lenses as reported by Kock were limited to one polarization. Therefore, a further improvement was to combine rows of vertical parallel plates with stacked horizontal plates, yielding to an eggcrate structure [4], which also provides a more robust assembly.

A new surge of interest in artificial effective media recently followed the so-called split-ring resonator (SRR) [5]. By overlapping the negative magnetic behavior of this particle with a negative electric permittivity media such as a wire mesh array, a revival of the left-handed media (LHM) proposed by Veselago [6] in the late 60's of the last century was attainable. Among others, an intriguing property of LHM is negative refraction which comes as a result of the Negative Index of Refraction (NIR) of these media.

The major consequence of the negative refraction regarding lens issue is that a slab of thickness t, made of a LH metamaterial with $n = -1$ can focus in a focal point the radiation of another point source located at a distance $l < t$ from the slab, see [6]. Moreover, shaped metamaterial lenses behave as the mentioned metallic TE-lens does: when the refractive index n is either negative or positive but less than 1, plane wave focusing can be achieved using plano-concave lenses, in contrast to the convex profile needed for ordinary $n > 1$ dielectrics. Continuing with the comparison, it is worth mentioning that for the same focal length a larger radius of curvature is allowed with negative index of refraction metamaterials, and thus, metamaterials lenses are thinner and aberrations may be minimized [7]. Furthermore, since the double-resonance scheme for achieving LHM allows, in principle, independent control of the electric permittivity, e, and the magnetic permeability, m, it is possible to obtain $n = -1$ maintaining the normalized characteristic impedance equal to 1, $\eta = (\mu/\varepsilon)^{1/2} = 1$, a feature that happens when both permittivity and

permeability are e = m = -1. Therefore, the compromise between low reflection and thickness can be overcome by this approach.

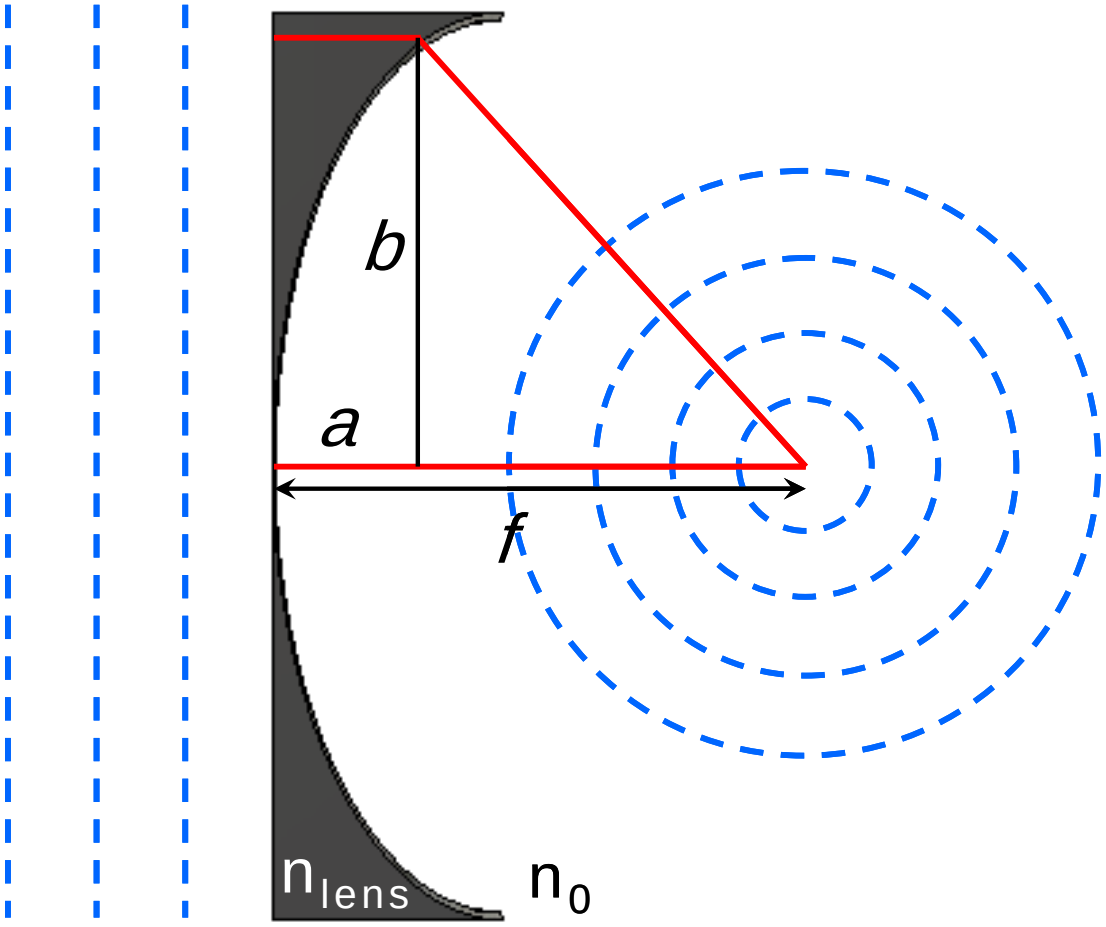

Fig. 1. Schematic of a lens that focuses a plane wave or transforms a cylindrical wave-front into a plane wave.

However, there is more to the story. In a first approximation, an ideal (i.e. lossless) slab of LHM with $\varepsilon = \mu = n = -1$ is actually a perfect lens [8] (reformulated as near-perfect lens because of the singularity arisen when ε and μ are exactly equal to -1 [9]). And this fact has become one of the main driving forces in metamaterials along with the quest of a low-loss metamaterial in the visible range. The fabrication of metamaterials using a pair of subwavelength hole arrays drilled in very thin metallic plates [10,11], termed fishnet structure, has become the most promising scheme at optical wavelengths. In the millimeter wave range, similar results have been observed [12]. Indeed, losses have been further minimized due to the use of properly engineered stacked subwavelength hole arrays under Extraordinary Transmission (ET) [13,14]. This structure presents negative refraction as it has been shown in a straightforward pure geometrical and experimental work [15].

The next step in ET-based metamaterials has been the characterization of the foci of a plano-concave parabolic NIR metamaterial lens operating at millimeter wavelengths composed of stacked subwavelength hole arrays patterned in aluminum plates [16]. Moreover, a bi-concave lens has been reported following

the same route [17]. This LH Extraordinary Transmission lens, LHET-lens, resembles the eggcrate lens, but the physics is completely different since the former works in the cut-off region of the circular waveguide determined by the stacked subwavelength holes whereas the latter deals with modes in propagation. Finally, it is worth mentioning that negative refraction lenses with constant or gradient index have been constructed by employing other metamaterial topologies or photonic crystals [18-20].

In this work we provide a further analysis of LHET-lenses, providing a comparison with metallic lenses. The frequency dependence of the focus of both bi- and plano-concave LHET-lenses is measured. Furthermore, we show the angular dependence of the antenna formed by an open-ended waveguide source and a plano-concave lens. All these results are recorded along E- and H-plane, *y-z* and *x-z* planes respectively.

Thus, this work complements previous publications by including: a comparison with old metallic lenses, highlighting similarities and differences; a full band characterization of the focal chromatic aberration of both plano-concave and bi-concave lens, instead of particularizing to a single frequency as in [16, 17]; experimental focus detection employing horn antennas and open-ended waveguides for the bi-concave lenses; of importance for the antennas community is that we present for the first time the angular power distribution (co- and cross-polar) of the plano-concave lens along with a characterization of its matching.

Finally we will consider the response of the LHET-lens when the effective negative index of refraction approaches zero. One of the main advantages of Near Zero Metamaterial (NZM) lenses is that ohmic losses are expected to be negligible because we are far from the resonant frequencies of the Drude and Lorentz responses of the electric permittivity and magnetic permeability, respectively. Moreover, given its ability to tailor both ε and μ, the NZM lens can also potentially be free-space matched.

METHODS, ASSUMPTIONS, AND PROCEDURES

Although not always strictly accurate, the easiest way to grasp the profile of generic lens is to look at Fig. 1 and apply ray tracing analysis. By enforcing equality between electrical path lengths of a general ray and a ray that crosses the lens through its principal axis, we get the following relation:

$$\sqrt{(f-a)^2+b^2}\cdot n_0 + a\cdot n_{lens} = f\cdot n_0 \quad (1)$$

where f is the distance between the focus and the lens, and n_0 and n_{lens} the index of refraction of the air (n_0 = 1) and the lens respectively. By rearranging terms,

$$\left(1-n_{lens}^{\ 2}\right)a^2 - 2\cdot f\cdot\left(1-n_{lens}\right)\cdot a + b^2 = 0 \quad (2)$$

which is the expression of the locus of an ellipse. The specific profile depends on the index of refraction. In general, the profiles obtained are ellipses or hyperbolas, regardless the sign of n. A case of particular interest is when n_{lens} = -1 (its positive counterpart is obviously trivial), in which the equation simplifies to $b^2 = 4\cdot f\cdot a$, and the profile is parabolic. Curiously, in geometrical optics an index of refraction n = -1 has been used as a mathematical tool to describe the reflection at the interface between air and a metal [21], which particularized to parabolic-shaped mirrors leads to the well-known property of focusing parallel rays on a point called focus of the parabola.

The advent of LH metamaterials made it possible the fabrication of a true media with index of refraction n = -1. Therefore, such parabolic-profiled media refract (i.e. transmit) the ray rather than reflecting it, and thus, allow the possibility to work in transmission. In the particular case when there is impedance matching between the two media ($\varepsilon = \mu$ = -1), waves can go through the surface without any reflection [6,22]. Finally, for other values of n < 0, the general shapes deduced from Eq. 1 are ellipses and hyperbolas.

On the other hand, previous metallic lenses designs do not consider negative parameters and the profiles employed are ellipses or hyperbolas, but never parabolas. For instance, Kock's lenses can be sorted into two main categories: TEM- and TE-lens. When an electromagnetic wave is polarized perpendicular to the plates, the waveguide formed by the plates supports a TEM mode. On the other hand, when the electric field is parallel to plates, the first propagation mode is TE_1.

In the case of the TEM-lens [3], the phase velocity in both media, air and parallel plates waveguide, is identical. So, in order to change the electric path length compared with free space, plates are bent as meanders or tilted to force an angle with the direction of propagation, and increase the physical path length.

TE lenses [2] provide more degrees of freedom because the phase velocity between the waveguide and free space is different and then the electric path is also different. As shown in [2] the index of refraction is between 0 and 1 unlike dielectric materials, whose index of refraction is always positive and greater than 1. Again, concave and convex lens change its role as a consequence of having $0 < n < 1$.

Once we know the profile required for a lens whose index of refraction is n = -1, we concentrate our effort in finding the frequency at which our LHET

metamaterial exhibits this index, although this does not necessarily involve matching to free space as stressed in the introduction. To this end, the dispersion diagram of the infinite structure is firstly calculated by using the eigenmode solver of the Finite-Integration Time Domain commercial software CST Microwave Studio™. Let us take the unit cell and apply periodic boundary conditions with specific phase shift across the cell in the longitudinal dimension, i.e. the stacking direction, whereas in the cross-sectional dimensions electric and magnetic walls are employed. The electromagnetic wave propagating in this artificial waveguide, thus, resembles the one of a TEM plane wave [23]. The unit cell parameters are: hole diameter h = 2.5 mm, transversal lattice constants d_x = 3 mm and d_y = 5 mm, longitudinal lattice constant d_z = 1.5 mm (~0.27l), and metal thickness w = 0.5 mm. We use doubly periodic subwavelength hole arrays to reduce the size of the lens [24] assuming the penalty of polarization dependence. We have modeled the metal as a perfect electrical conductor (PEC), which is a reasonable approximation for metals at millimeter-waves. For this particular set of parameters, ET emerges, for a single plate, around 57 GHz despite the individual hole starts to propagate at 70 GHz, that is, the cut-off frequency of the circular waveguide defined by the hole. From the dispersion diagram, the effective index of refraction is directly calculated through the relation:

$$n = \sqrt{\varepsilon\mu} = \frac{c}{v_p} = c\frac{k}{\omega} \tag{3}$$

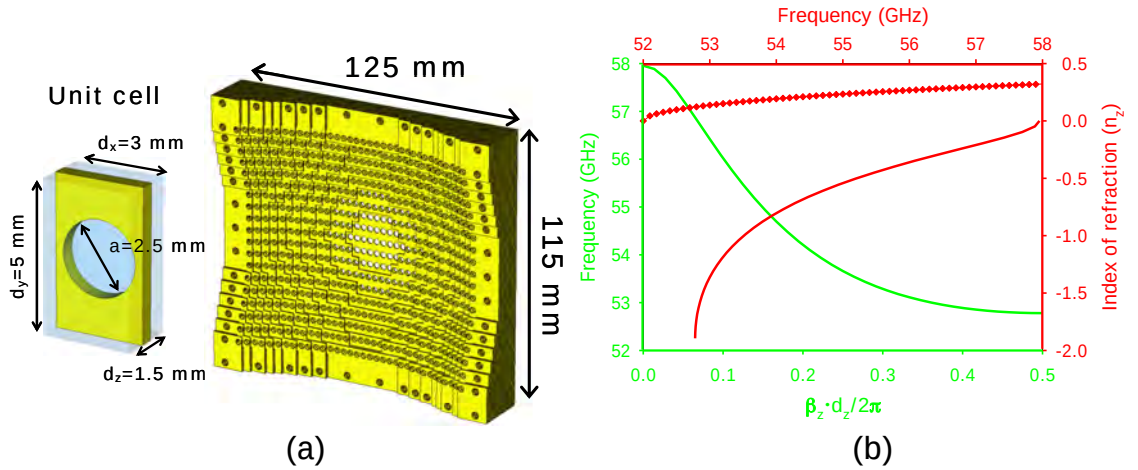

Fig. 2. (a) Sketch of a planoconcave lens, and details of the unit cell (inset). (b) Analytical dispersion diagram (green) of an infinite structure made of stacked sub-wavelength hole arrays, whose unit cell parameters are: transversal lattices d_x = 3 mm, d_y = 5 mm, longitudinal lattice constant d_z = 1.5 mm, hole diameter h = 2.5 mm, and metal thickness w = 0.5 mm. Corresponding index of refraction associated to this LH mode (red), and index of refraction of the first propagation TE mode supported by parallel metallic plates with separation between plates d = 2.9 mm (cut-off frequency f_{co} = 52 GHz (red diamonds).

Both, first propagation mode of the dispersion diagram and its corresponding index of refraction are plotted in Fig. 2. Clearly, the mode of the stacked subwavelength hole array structure remains below the cut-off frequency of the hole and presents negative slope, i.e. phase velocity opposite to the group velocity. On the other hand, this frequency response predicts an index of refraction n = -1 at 53.5 GHz. The inherent frequency variation causes

dispersion in the structure which limits its bandwidth and causes chromatic aberration as TE-lenses do. The index of refraction of a TE-lens with cut-off frequency f_{co} = 52 GHz, that is, d = 2.9 mm, is also depicted in Fig. 2 for comparison purposes. In terms of bandwidth and chromatic aberration usual metallic lenses may have better performance. A more thorough analysis would include the dependence of n on the angle of incidence; however, this is beyond the scope of this paper, since, as shown below, the conclusions drawn from Fig. 2 match well with the measured results. This is due to the fact that refraction is governed by the lens profile and axial backward propagation, as happened in our previous wedge experiment [15]. For a more complete two-dimensional analysis, see Refs. 25 and 26.

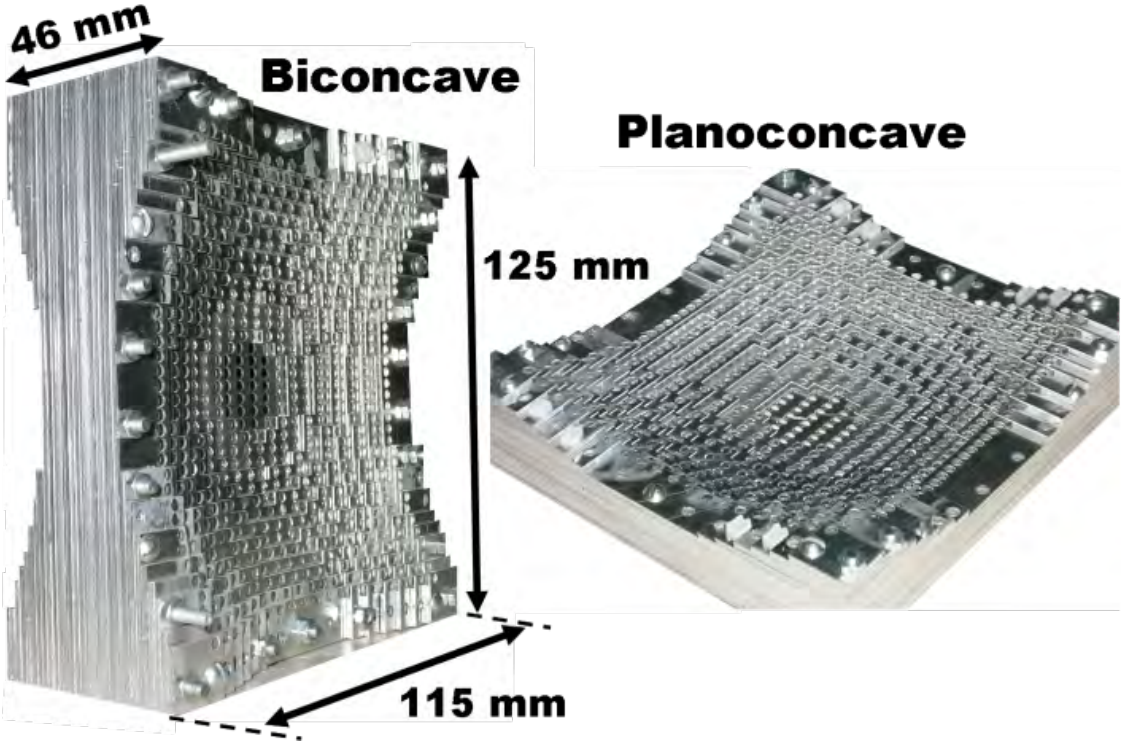

Fig. 3. Pictures of the prototypes: (left) bi-concave LHET-lens; (right) plano-concave LHET-lens. Unit cell parameters are: transversal lattices d_x = 3 mm, d_y = 5 mm, longitudinal lattice constant d_z = 1.5 mm, hole diameter h = 2.5 mm, and metal thickness w = 0.5 mm.

Following previous discussion, a bi- and plano-concave LHET-lens working at 53.5 GHz is constructed with focal length f = 50 mm (8.9l), i.e., the focus is centered at a distance of 27 mm from the nearest transversal plane of the lens. The 3D lens is generated by revolving the parabola defined by $x^2 = 200 \cdot z$. We approximate the smooth parabolic shape with a staircase profile with step equal to the size of the cross-section dimensions of the unit cell of the subwavelength hole array. This fact limits the sharpness of the foci when we illuminate the plano-concave lens with a plane wave, as it will be apparent in the experimental results shown below. The bi-concave lens is constructed by simple placing back to back two identical plano-concave lenses.

The whole structure, including the frame for the assembly, has maximum dimensions of 125 mm × 115 mm × 23 mm (46 mm) for the plano-concave (bi-

concave) lens, see Fig. 3. These dimensions along with the design focal length ensure a negligible spill over.

Finally, experimental results are recorded with an ABmm^{TM} Quasioptical Vector Network Analyzer within the V-band of the millimeter-wave range (45 to 70 GHz). This instrument is based on a solid state multiplier that generates the millimeter-submillimeter wave frequencies which are detected by harmonic mixer heterodyne downconversion. The particular experimental set-up for each LHET-lens, namely bi- and plano-concave, is described in each section, since the illumination is changed in each case.

For the case of the NZM lens, we have to take in account that the incidence of an electromagnetic wave into a médium with an effective index of refraction near zero (without loss of generality, the first medium is air, $n_{air} = 1$), Snell's law imposes the restriction of angles of incidence close to 0^o in order to have transmission. Thus, the ideal profile in this case would be a hemispherical Shell, [21 and 7]. Note that according to Fermat's principle and the related concept of optical path, a lens whose index of refraction is lower than the surrounding medium ($n_{lens} < n_{medium}$ and considering also negative values) must have a concave profile in order to transform a spherical wave front to a plane wave and vice versa, [21 and 7]. This case is different from the ε -near-zero materials, where any arbitrary shape can be used at the input to obtain a plane wave at the output as long as polarization is TM and the output face is plane [27]. However, considering that our lens has a small numerical aperture, its parabolic profile can approximate reasonably well the ideal one. (Indeed, any lens profile at small angles is approximately the same as a hemispherical Shell, [7]).

RESULTS AND DISCUSSION

Initially, we explore the question of point source. To illustrate the effect of the illumination, we compare results between corrugated horn antenna and open-ended rectangular waveguide illumination. To this end, we place firstly the prototype in the path between a transmitting corrugated horn antenna and an identical one acting as receiver. The transmitting antenna launches a linearly polarized Gaussian beam [28], whose E-field is along the large transversal periodicity d_y, of the structure. The distance between the sample and the transmitting antenna is 45 mm (experimental position of the focal length [17]), whereas the receiving antenna scans the transmission coefficient for four different distances along the principal axis of the lens, z = 35, 45, 50, 75 mm. Thus, these values along with the dimensions of the lens given at the end of the preceding section, imply that we are working in the radiating near-field, since $0.62\cdot(D^3/\lambda)^{0.5} \approx 370$ mm, where D is the largest dimension of the paraboloid [28]. The calibration is done by recording the transmission coefficient at each distance when the LHET-lens is not in the way.

The results are plotted in Fig. 4 (a). Frequency filtering behaviour (transmission passband centered at the LHET frequency) and Wood's anomaly (at 60 GHz) aside, it should be noted that lens effect is not observed since the transmission coefficient does not exceed calibration, although, at least, a relative higher transmission is scanned for distances around z = 45 mm. Quite a different scenario arises if we replace corrugated horn antennas by open-ended rectangular waveguides. This feed provides much less directive illumination, i.e. a broader pattern although slightly asymmetric both in E- and H-plane. From now on, we will use open-ended rectangular waveguides as feeder and detector in this section. With this set-up, a transmitted power enhancement of 11 dB at 54.2 GHz appears for the conjugated point of the source at the image zone, that is, z = 45 mm, see Fig. 4 (b). Moreover, this enhancement is not only caused by the collimation associated with the subwavelength hole array [29] but mainly due to the lens profile, since one perforated aluminium plate presents only 3 dB enhancement at 54.2 GHz, pink curve in Fig. 4 (b).

Subsequently we generate maps of power lateral distribution as a function of frequency and transversal position. The transmitting antenna remains fixed at 45 mm, whereas the receiving antenna is moved transversally at three different distances z = 30, 45 and 75 mm in order to scan the power in both planes x-z (H-plane) and y-z (E-plane) planes. In Fig. 5, clear filtering is observed, which is caused by the LHET-lens in the three cases. Besides, H-plane presents higher sidelobes than the E-plane for the whole ET band. This is in accordance with the simulation results of Ref. 17.

From panels 5(b) and 5(e), the spatial resolution at 54.2 GHz determined by the distance between the peak and the location of the first null can be measured. In the E-plane, the resolving power is 0.77λ, whereas in the H-plane the value is 1.35λ. Recalling that the Rayleigh criterion for a circular lens of diameter D_l defines the spatial resolution as $\Delta = 1.22\cdot\lambda\cdot f/D_l$, it is worth noting that the experimental resolution of our proposed lens in the E-plane is close to the theoretical value for a dielectric lens with a focal length-to-diameter ratio f/D similar to our bi-concave LHET-lens, despite the employed non point source.

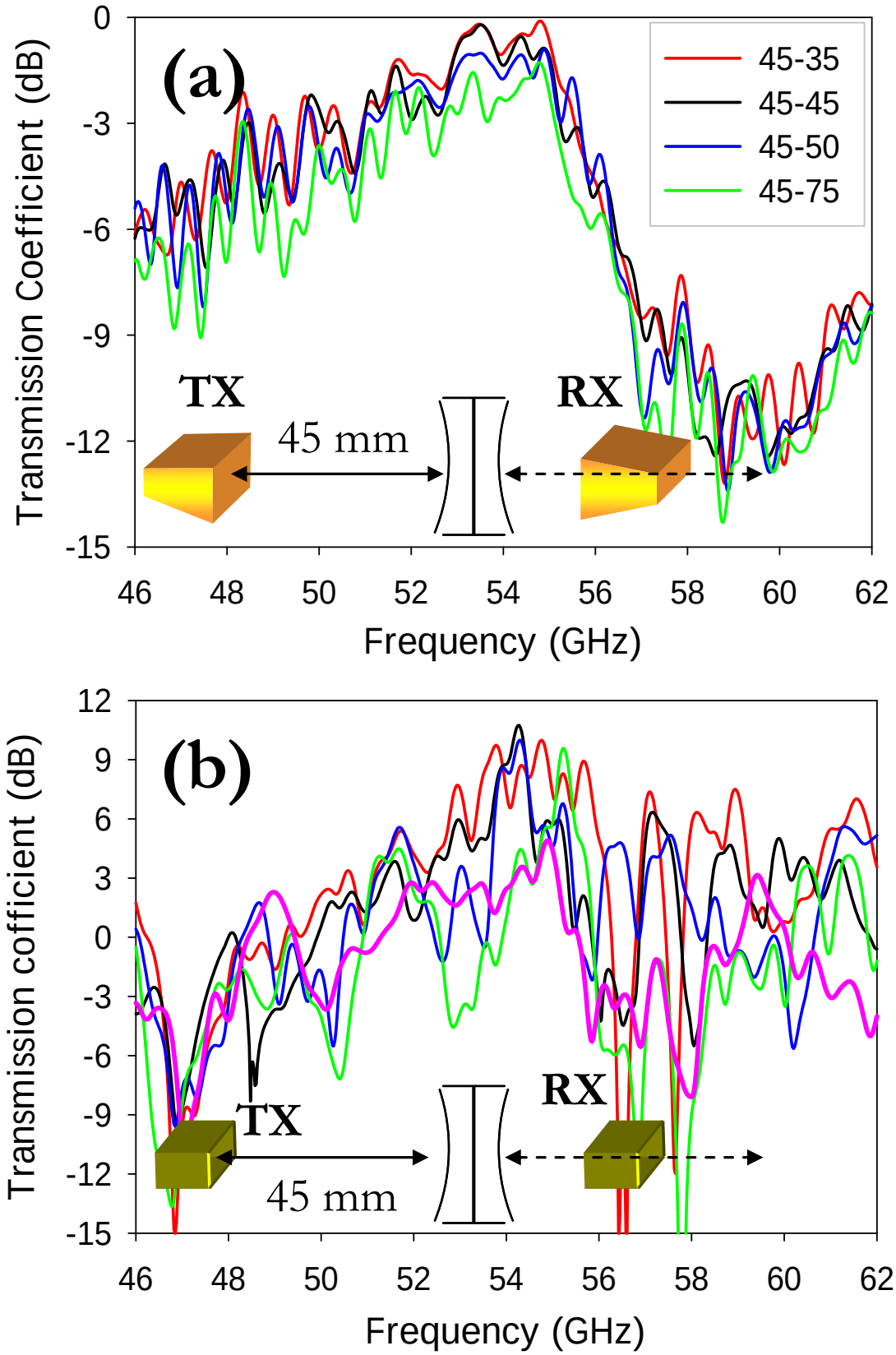

Fig. 4. Transmitted power recorded when the lens is illuminated by (a) corrugated horn antenna and (b) open rectangular waveguide. Besides, (b) transmitted power through a doubly periodic subwavelength hole array plate (pink curve). Insets of each figure sketched the experimental set-up used.

On the other hand, the longer transversal length of the source along *x* may be the reason of the deterioration of the spatial resolution along this axis.

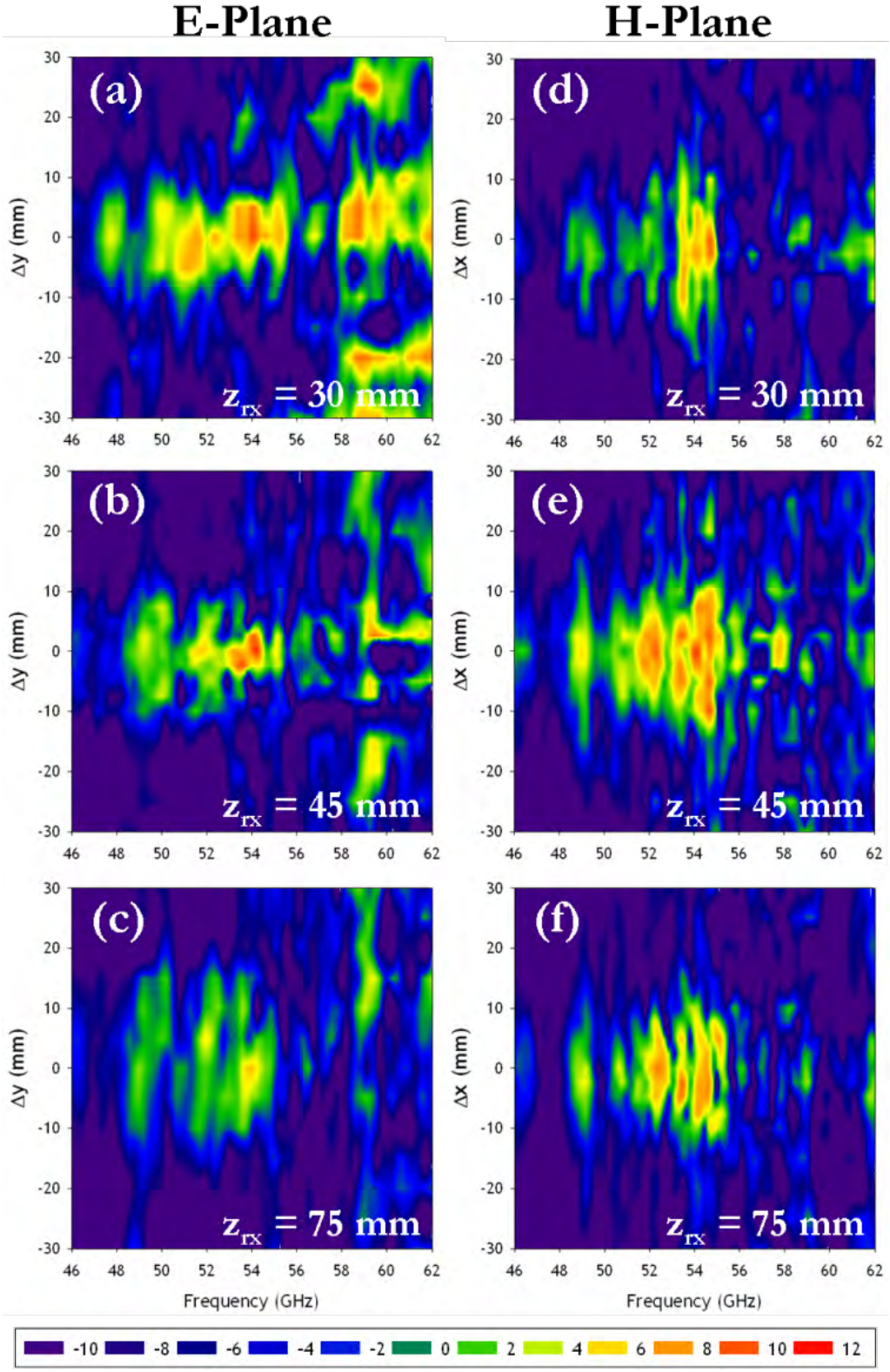

Fig. 5. Measured lateral power distribution (dB) as a function of frequency for E-plane (a)-(c) and H-plane (d)-(f) at three different distance of the image plane, *z* = 30 mm (a) and (d); *z* = 45 mm (b) and (e); and *z* = 75 mm (c) and (f). Excitation and reception was done using open waveguides.

Firstly, we will study the case of plano-concave lenses. In Ref. 16 we showed the asymmetrical focus at 53.5 GHz of our plano-concave LHET-lens and it was tentatively attributed to the larger step in the staircase approximation of the parabola along the *y*-direction. Now, we investigate in more detail this asymmetrical focus vs. frequency, as well as the cross-polar behavior of the lens.

A schematic of the experimental set-up can be found on top of Fig.6. The LHET-lens is illuminated from its flat back face by a Gaussian beam [28] generated by the corrugated horn antenna. For the dimensions of the experimental set-up, when the Gaussian beam reaches the LHET-lens, it is expanded enough so as to consider the illumination as a good approximation to a plane wave. The normalized lateral power distribution relative to the absolute maximum of each panel is shown in Fig. 6 for the two principal cutting planes, that is, E- and H-cutting planes, on the left and right column of the figure respectively. The mentioned asymmetry between planes is still present for the whole frequency range. Moreover, it seems that at the expected focal plane z = 45 mm, the beam is more collimated within the ET band, although the difference is far from obvious. This fact somehow reveals that chromatic aberration is not as severe as it was expected from the dispersion diagram.

We also scanned the cross-polarization, depicted in Fig. 7. As previously, left column presents E-plane measurement, whereas on the right one is depicted the H-plane and, as usual, graphs have been normalized to the absolute maximum of each corresponding co-polar measurement. The cross-polar component along the principal axis of the lens has a value 30 dB below the co-polar measurement within the whole frequency range (50-59 GHz). This negligible magnitude is slightly increased at transversal positions of ± 5 to 10 mm in both planes. However, these side lobes appear at frequencies higher than 56 GHz, i.e. beyond the design frequency.

To analyze in depth the origin of the asymmetry, we embarked on a 3D full-wave numerical analysis of the real prototype; see Fig. 2(a). A plane wave is launched from the flat face of the plano-concave lens and the power distribution is recorded along the E- and H-plane at the focus. The numerical results are plotted in Fig. 8. From that plot we appreciate an almost symmetric focus along both planes and this, in principle, disagrees notably with experimental results. In previous papers [16, 17] we explained this by simply stating that the cause could be the different step in each direction. This is only partially true, since another reason for the incongruity between numerical and experimental results relies directly on the experimental hardware. Since our receiver is not subwavelength in size (it is a corrugated horn antenna), it performs an integration of power along its effective area. On the E-plane, the lateral lobes (the other key ingredient) caused by large lattice constant along *y* (of the order of wavelength), cannot be resolved, and thus, in the experimental results they contribute to the central spot recorded by enlarging the focus dimensions. In a first approximation we have estimated the integration length as the effective length of the receiver antenna. The numerical values calculated under this assumption are also plotted in dashed lines in Fig. 8. Notice that the cutting planes are now asymmetric, in good agreement with the experiment.

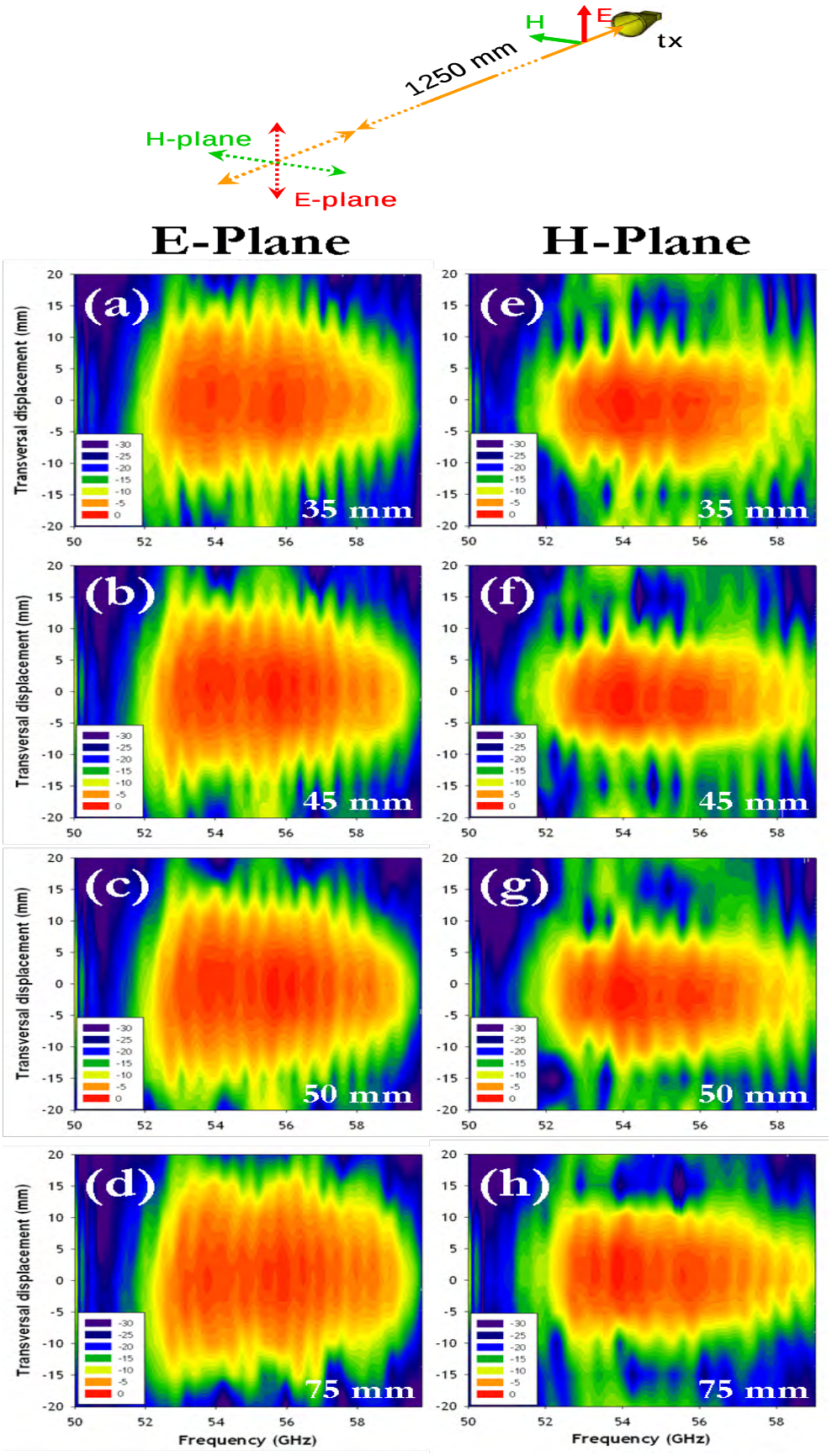

Fig. 6. Co-polar measurements of lateral normalized power distribution as a function of frequency for E-plane (left column) and H-plane (right column) at four different distance of the image plane, z = 35, 45, 50 and 75 mm. Excitation and reception was done using corrugated horn antennas.

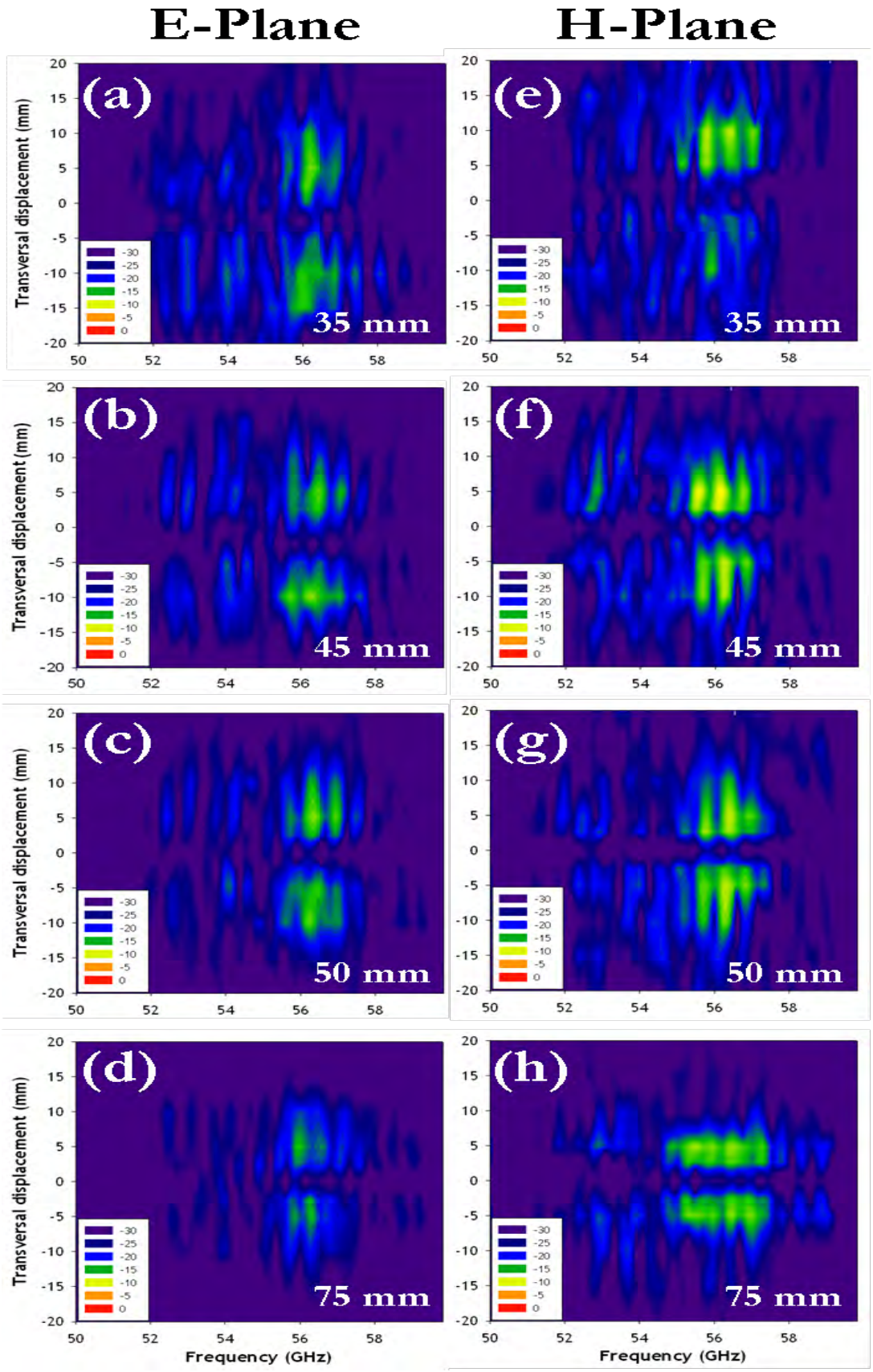

Fig. 7. Cross-polar measurements of lateral normalized power distribution as a function of frequency for E-plane (left column) and H-plane (right column) at four different distance of the image plane, z = 35, 45, 50 and 75 mm. Excitation and reception was done using corrugated horn antennas.

The full-width at half maximum in the E-plane is 31 mm in the experiment and 30 mm in the corrected simulation. The values for the H-plane are less accurate being 22 mm and 9 mm respectively. This last discrepancy is probably a consequence of integrating only in one dimension instead of performing a surface integration.

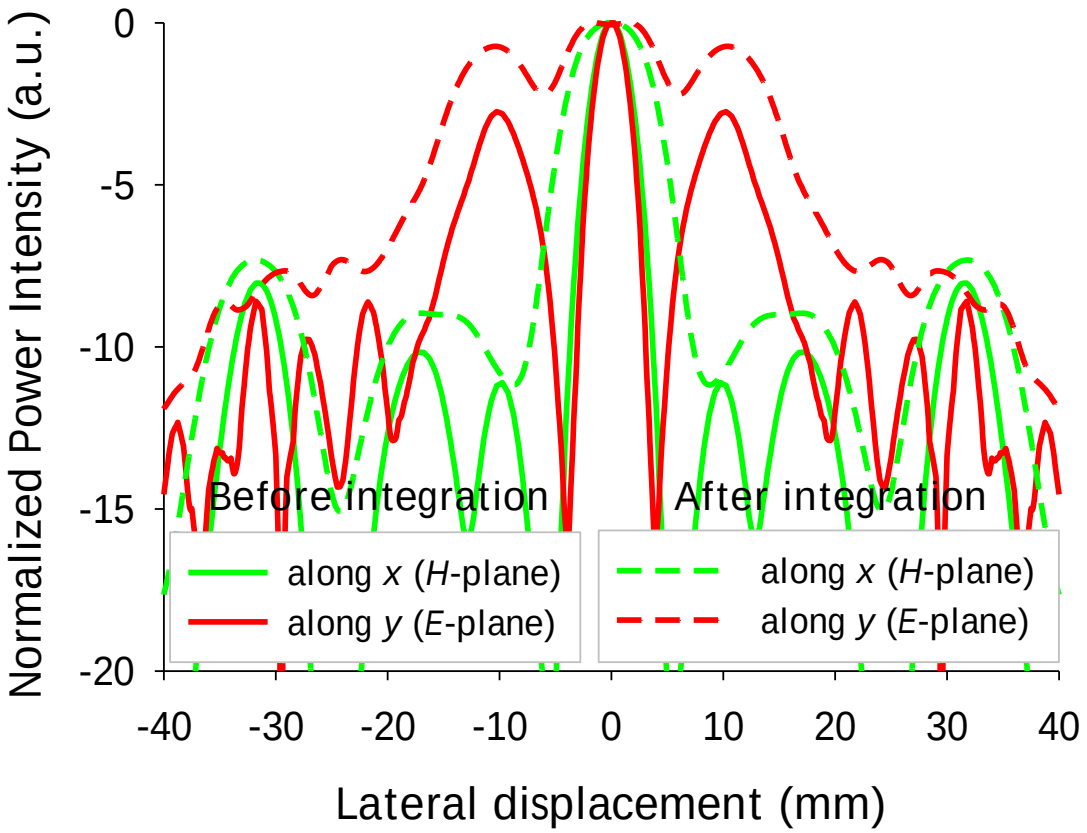

Fig. 8. Simulation results of the power distribution along *x* (green line) and *y* (red line) for *f* = 53.5 GHz. Dashed line is the result after carrying out an integration to emulate the experiment with a horn antenna.

The final step is to characterize the radiation pattern of the lens+antenna assembly. In the origin of metallic lenses, this was the principal aim for their development. Therefore, a qualitative contrast between our plano-concave lens and an eggcrate lens is worth.

To this purpose, we run two simulations employing the transient solver of CST Microwave Studio™ for each structure – classical eggcrate and our plano-concave lens – particularized to the reduced case of two-dimensional equivalents, due to computation constraints. The 2D structures are illuminated by a dipole (point source) and the unit cell parameters those of the plano-concave LHET-lens, whereas eggcrate unit cell parameters have been chosen as similar to those values as possible for fair comparison; namely: $d_x = d_y = 3$ mm, square hole size $h_{eggcrate} = 2.9$ mm (square waveguide), and focal length $f_{eggcrate} = 50$ mm. For this particular set of parameters, the eggcrate lens design imposes a limit in the size of the lens of $19 \cdot d_x$ according to Eq. 2 (ellipse), and thus, the LHET-lens is designed with this constraint as well. Also, the

transversal dimensions ensure monomode operation (only the fundamental TE_1 mode is above cut-off in the waveguide).

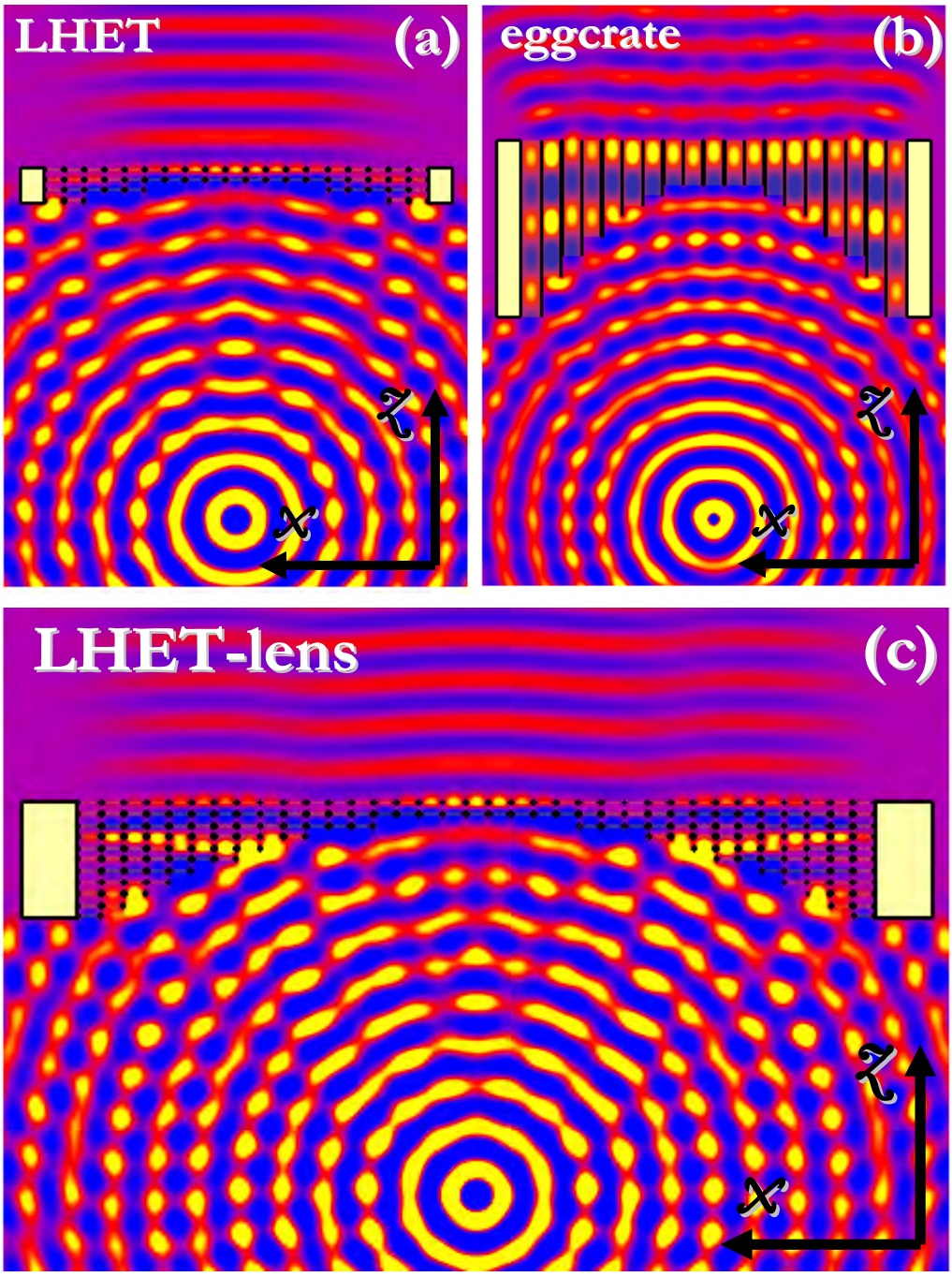

Fig. 9. Simulated electric field E_y for LHET-lens antenna (a) and eggcrate-lens antenna (b) with identical unit cell and total transversal dimensions for comparison purpose and excited by a dipole. (c) Idem for LHET-lens antenna with dimensions of fabricated prototype.

For a reasonable compromise between reflection loss and thickness, the effective index of refraction is taken $n_{eggcrate}$ = 0.5, and then, the frequency is 59.7 GHz. Electric field of both simulations along with the simulation of real LHET prototype are plotted in Fig. 9. Note that for this configuration, the eggcrate is illuminated by the source under an angle of around 87 deg.

After the qualitative numerical work, we compare some radiation pattern parameters between eggcrate configuration and LHET-lens, also extracted from the simulation. From Fig. 9 one can observe that the cone of rays impinging on each structure is different. Thus, let us then compare an eggcrate consisting of 19 waveguides with two LHET-lenses: the first one is composed of 19 holes, which implies an angle of illumination much lower than 87 deg. The second analyzed LHET-lens has identical angle of illumination by the primary source as the eggcrate. This latter LHET-lens requires then 27 holes (that is, the total width is $27 \cdot d_x$) so as to have an angle of radiation cone of around 87 deg as the eggcrate. Table I summarizes half-power beamwidth (HPBW), first null beamwidth (FNBW) and first side lobe level (FSLL) for the three configurations along the H-plane. In terms of FSLL LHET-lenses give better performance than eggcrate lens, whereas for improvements in HPBW and FNBW characteristics, it is necessary to design a LHET-lens with a similar cone of illumination as the eggcrate lens, which increases the physical aperture of the LHET-lens whereas the eggcrate is much thicker at its boundaries. Apart from electromagnetic considerations, there is another feature which makes LHET-lenses be a powerful alternative to eggcrate lenses: the weight. Due to the plate-air gap assembly, the metal is reduced and so is the weight of the LHET-lenses.

TABLE I
radiation pattern parameters along h-plane

	Eggcrate	LHET-lens 19 holes	LHET-lens 27 holes
HPBW	4.4 deg	8.4 deg	4 deg
FNBW	10 deg	16 deg	10 deg
FSLL	9 dB	14.3 dB	15.2 dB

From now on, we focus on the experiment of our plano-concave LHET-lens. The source, an open-ended waveguide, is fixed at the focal spot at 45 mm from the lens vertex, and the detector, a corrugated horn antenna at z = 1900 mm. Due to the concave-profiled face of the lens, the lens has a higher efficient aperture than dielectric lenses because the parabola admits a bigger cone of rays than a convex surface. A schematic of the experimental set-up is shown in Fig. 10, along with pictures of the real set-up. We estimate the minimum distance for the far field approximation to be valid at approximately $z_{ff} = 2 \cdot D^2/\lambda \approx 5680$ mm, where D is the diameter of the aperture [29]. Therefore, the angular power distribution measured here is only an approximation of the radiation pattern of the system composed of open rectangular waveguide source and plano-concave LHET-lens.

Since the ET Metamaterial forms a transversal array, it may be susceptible to grating lobes. With the double period, see Fig. 2, grating lobes appear within the ET band in the E-plane, but not in the H-plane. The explanation can be found by inspecting the relation for constructive interference of scattered electromagnetic waves emerging from a periodic structure: $d \cdot \sin\theta = m \cdot \lambda$, where d is the lattice constant of the grating, θ is the angle of emergence of the scattered wave with respect to the normal, λ is the wavelength of the electromagnetic wave, and m is an integer; one can infer that for a lattice

constant smaller than l, the equality cannot be fulfilled unless m = 0. Therefore, since the lattice constant along x-axis (H-plane) is smaller than l, whereas the lattice constant along y-axis (E-plane) is of the order of l, only the latter is susceptible of grating lobes within the ET band.

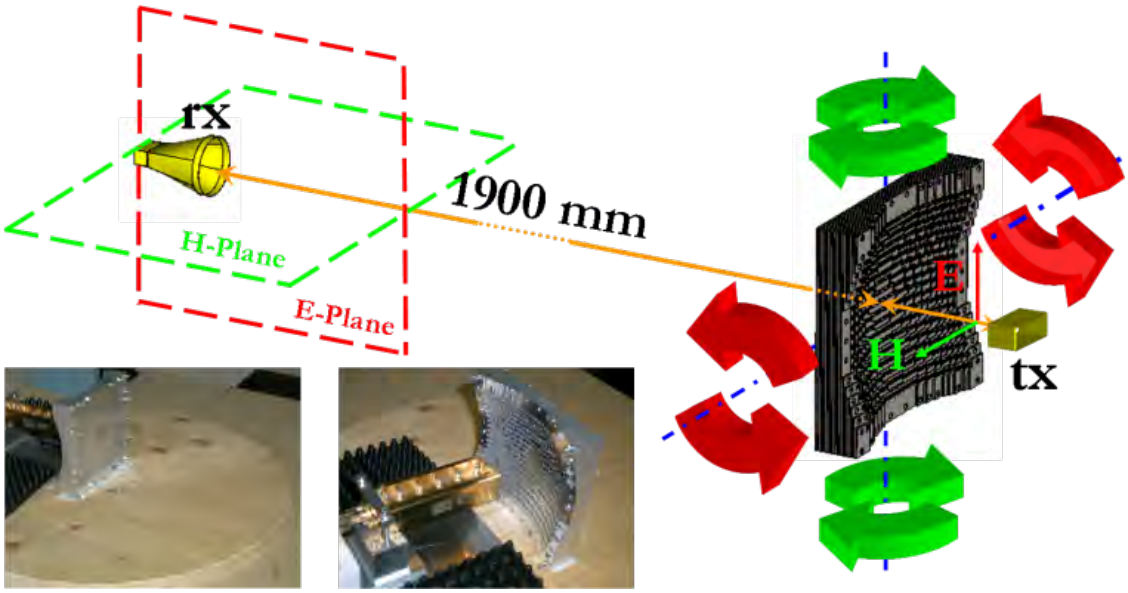

Fig. 10. Sketch of the experimental set-up for the angular pattern measurement of the set open-rectangular-waveguide-LHET-lens. (Insights) Pictures of the real set-up.

Experimental results in Fig. 11 corroborate this discussion. The enhancement at 54.2 GHz is 8.5 dB, whereas cross-polarization is -35 dB. E- and H-planes are different as it is usual in this kind of structures, since the currents excited at resonance go parallel to the electric field and explore more holes in that direction than in the orthogonal one [31].

The peak directivity calculated from the approximated formula Directivity = $4 \cdot \pi / (\theta_{-3dB,E\text{-}plane} \cdot \theta_{-3dB,H\text{-}plane})$ leads to 30.5 dB as a result of HPBWs of $\theta_{-3dB,E\text{-}plane}$ = 0.066 rad (3.8 deg) and $\theta_{-3dB,H\text{-}plane}$ = 0.169 rad (9.7 deg). This value is equivalent or even exceeds in some cases peak directivities of Fresnel zone plate antennas with comparable f/D [32]. From the directivity the effective area can be obtained, and from here the aperture efficiency can be calculated. We have an aperture efficiency of around 22%, which, in general, is better than typical numbers of Fresnel zone plate antennas of comparable f/D (around 10%) [33]. Standard metal lenses usually have higher aperture efficiency [2], but as mentioned above, our proposal has a lower profile which makes it competitive in terms of volume efficiency. In addition, enhancement up to 10 dB can be found at other frequencies close to this one with cross-polarization below 40 dB, but they were unexpected and the nature of them is still unknown. They may be caused by the fact that we are not in far-field conditions or by some experimental artifacts.

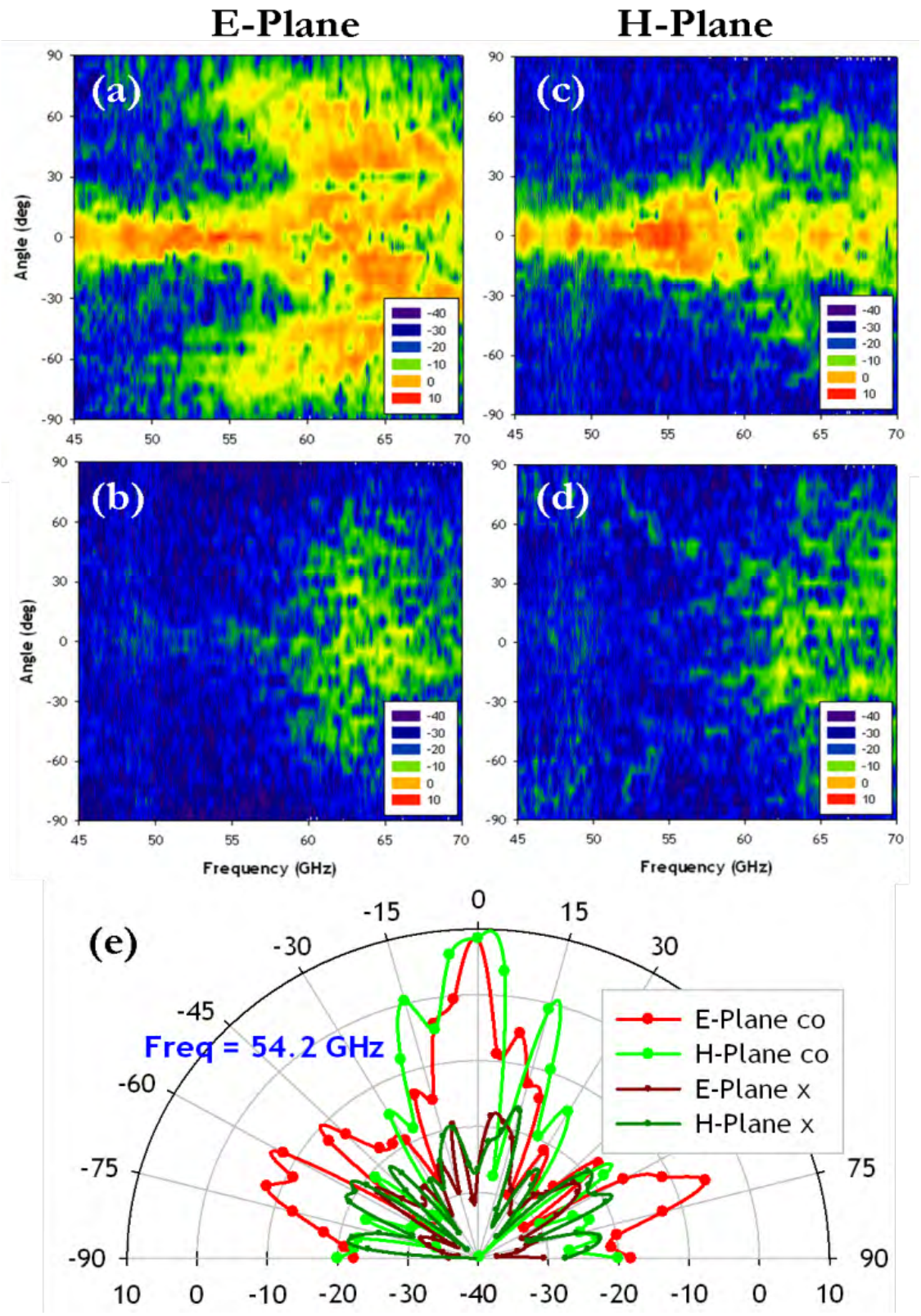

Fig. 11. Co-polar (top) and cross-polar (middle) measurements of the angular power distribution as a function of frequency for E-plane (left column) and H-plane (right column) under open-ended waveguide illumination. (Bottom) Cut-frequency at 54.2 GHz of preceding graphs. Excitation and reception was done using open waveguide and corrugated horn antenna, respectively.

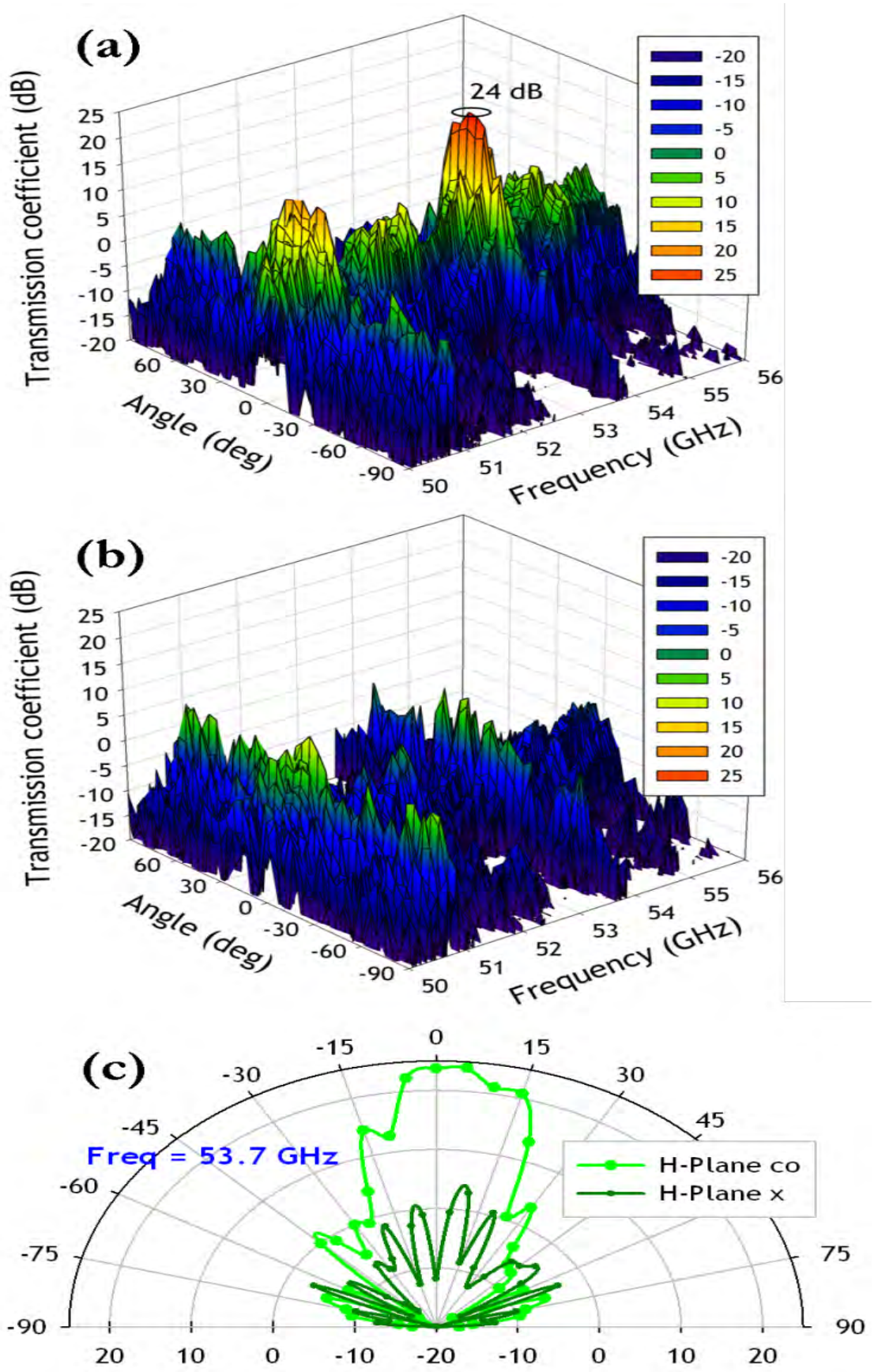

Fig. 12. Co-polar (top) and cross-polar (bottom) measurements of the angular power distribution as a function of frequency for H-plane when the feed is a resonant slot and receptor is a horn antenna.

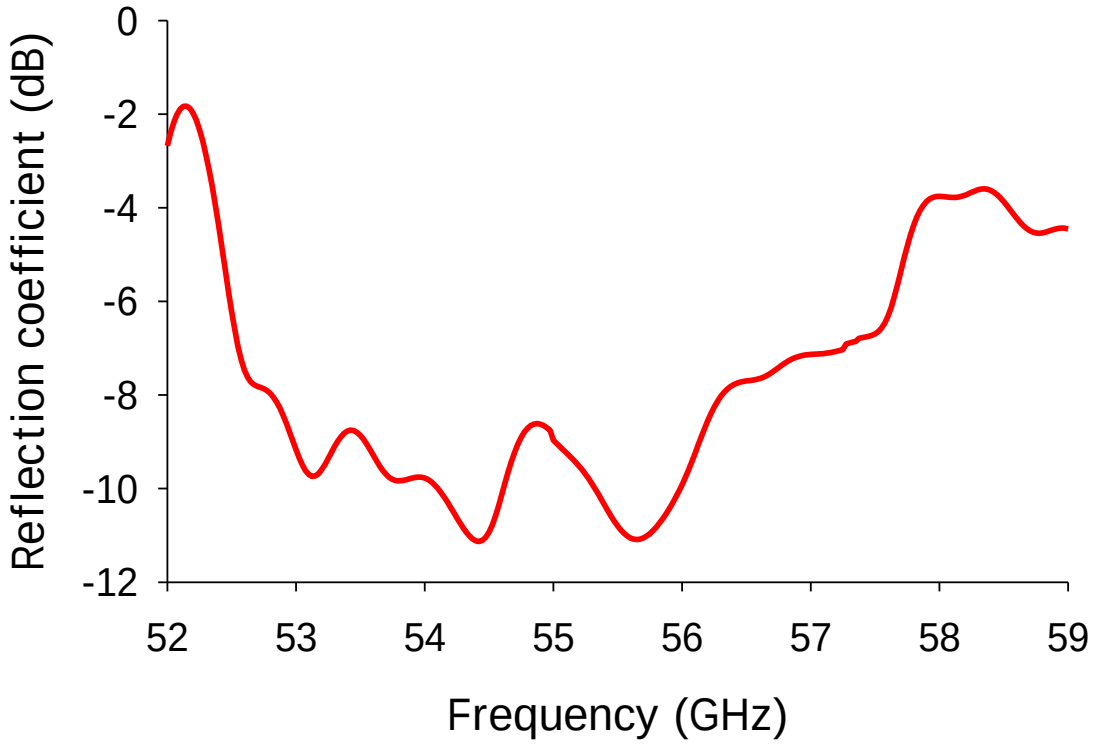

Fig. 13. Reflection coefficient of the LHET-lens antenna when it is illuminated by means of a corrugated horn antenna placed at the lens focus.

Now, we will consider the plano-concave LHET-lens illuminated by a resonant slot and a discussion about its matching.

Last but not least, as a further improvement of the feeding, we considered using a waveguide endeding in a resonant slot. The radiation pattern of this feed may be a better approximation to the point source in which the design is based. The experimental set-up is identical to the one sketched in Fig. 10, except for the source.

The angular power distribution along the H-plane, which is more interesting in terms of radiation since it does not exhibit grating lobes, is depicted in Fig. 12. Now, an enhancement around 23.9 dB is recorded in a narrow frequency band in the region of 53.7 GHz, close to the design frequency (53.5 GHz). This stresses the expected fact that there is a feeding-dependence in the frequency response. On the other hand, the cross-polarization remains below -30 dB with respect to co-polar around 53.7 GHz at the principal axes. Specifically, at 53.7 GHz in broadside direction, where the co-polar reaches its maximum of 23.7 dB (not that 23.9 dB is achieved at that frequency slightly moved to positive angles), the cross-polar has a value of -11.9 dB. As an approximation, if we estimate the half-power beamwidth in E-plane as before $\theta_{-3dB,E\text{-}plane}$ = 0.066 rad (3.8 deg), being $\theta_{-3dB,H\text{-}plane}$ = 0.288 rad (16.5 deg) in this case, the directivity is then 28.2 dB. Thus, the comments of the previous section linked to usual Fresnel zone plate antennas can be also brought here.

A final question to be discussed is that of the matching level that can be achieved with LHET-lenses. In this way, we have measured the reflection coefficient of the structure when it is illuminated by means of a corrugated horn antenna. In this way, we are sure that the matching level is good enough at the

output of the feeder and, therefore, the reflected power level will be detected with a reasonable dynamic range. On the other hand, as discussed previously, this illumination is not the optimal one for the LHET-lens. Anyway, looking at Fig. 13 one can observe that a value around -8 dB in the reflection coefficient can be obtained in a broad frequency band. This value can be considered as a worst case because of the employed experimental set-up.

Therefore, it follows that further research and optimization procedures are necessary to make possible the application of these new results in practical LHET-lenses. Anyway, the results of this section show the great potential of these LHET-lenses under a proper feeding for the design frequency.

Now, let's switch to the NZM lens experimental results. Figure 14 renders the angular distribution of the radiated beam in the H-cutting (xz) plane. A clear directivity enhancement (note that we are directly correlating the narrowing of the main lobe on one plane to an enhancement of the directivity, which, indeed, accounts for both planes) is recorded at λ = 5.24 mm (57.2 GHz). There is no other evidence of enhancement in the range between 5.12 and 5.30 mm, see Fig. 14(a). The cross-polar measurement (receiving antenna rotated 90◦ with respect to the incident vertical electric field) remains very low with respect to the copolar measurement as Fig. 14(b) shows. The origin of the cross-polar measurement may come from the modal nature supported by the circular hole since the fundamental mode (in cutoff because of the subwavelength dimensions) is the TE_{11} (Ref. 23), which displays some x component.

Therefore, a rectangular hole should reduce cross polarization because the fundamental mode is a TE_{10} without x component.

From Fig. 14(a) the maximum transmittance (main lobe) of the copolar component reaches a value of 27 dB (in linear scale, a factor of 500 times), improving previous experimental results on EBGs, [34,35]. Note that this happens at + 5º rather than at the optical axis [see Fig. 14(c)], where the value is 22 dB (a factor of 158), while the cross-polar measurement is 14 dB at +5º and has a maximum value of 18.5 dB at +10º [see Figs. 14(b) and 14(c)]. The slight displacement with respect to the optical axis may be due to an experimental misalignment.

The directivity enhancement at 5.24 mm is due to a refractive index approaching zero along with impedance matching, as demonstrated in Fig. 15. We have retrieved the constitutive parameters from the S-parameter simulation of two stacked layers (assuming small numerical aperture, the analysis of the lens can be reduced to its central zone) under normal incidence, see [36-38], and Fig. 15. As we are working at angles close to normal, this analysis can be considered a reasonable, yet evident, simplification because anisotropy [36-38] is disregarded. (The importance of anisotropy in the response will be shown in the next section.) Note that the values shown in Fig. 15 are just a mathematical interpretation. They model the response of the mesoscopic stack for a certain set of conditions, and its extension to truly effective values somehow lacks physics, [38,41,42]. For this numerical analysis, the electric conductivity of the aluminum was fixed to 3.72×10^7 S/m, and the problem was reduced to the unit cell with transversal periodic boundary conditions and solved with the frequency domain solver of CST Microwave Studio™ [43].

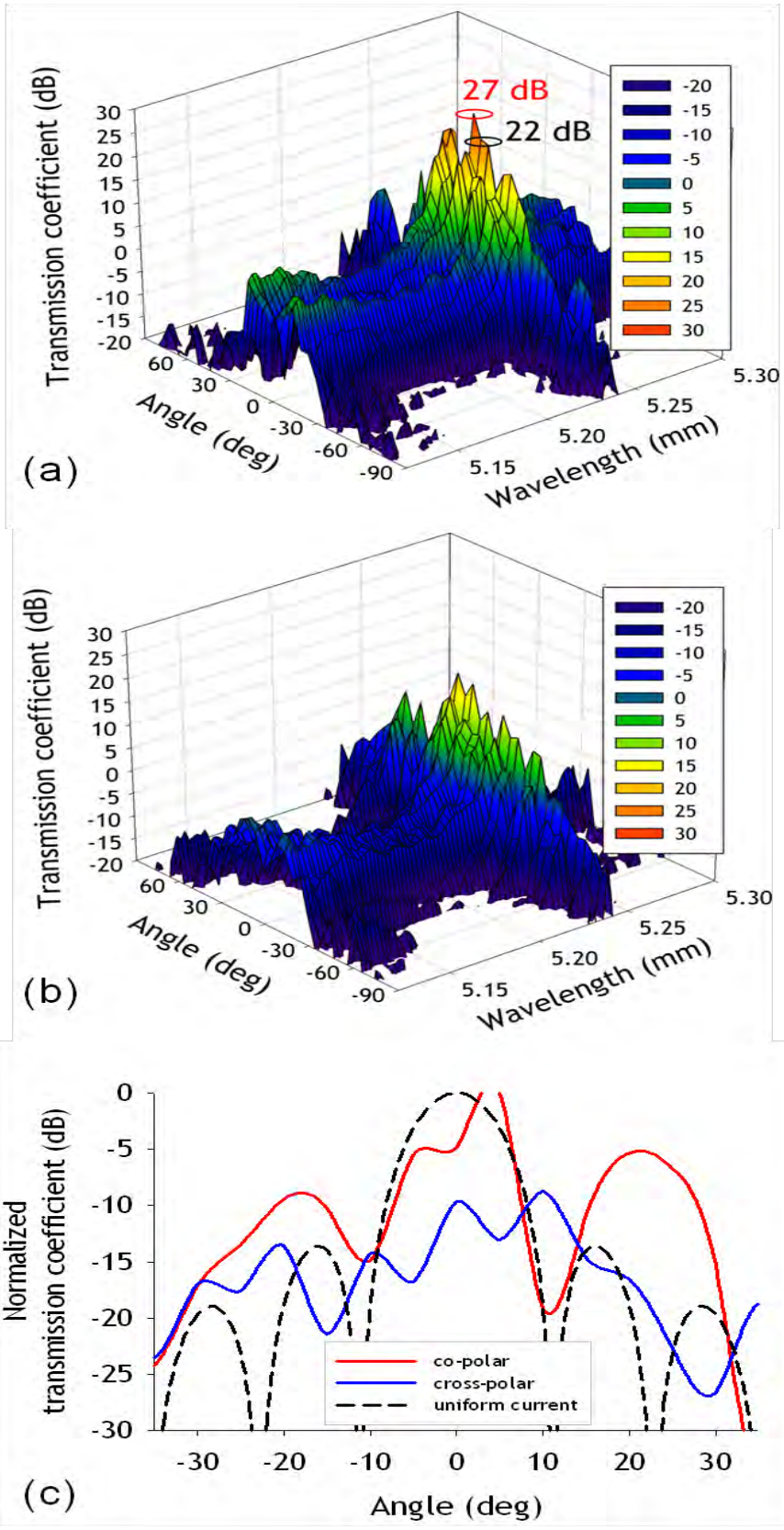

Fig. 14. Co-polar (a) and cross-polar (b) measurements of the angular power distribution as a function of frequency for H-plane. (c) Idem for the wavelength of maximum enhancement, red and blue curves, respectively. Normalized power pattern of a *x*-directed uniform line source with the same dimensions as the central part of our lens, that is, 9 holes × d_x = 27 mm (dashed curve).

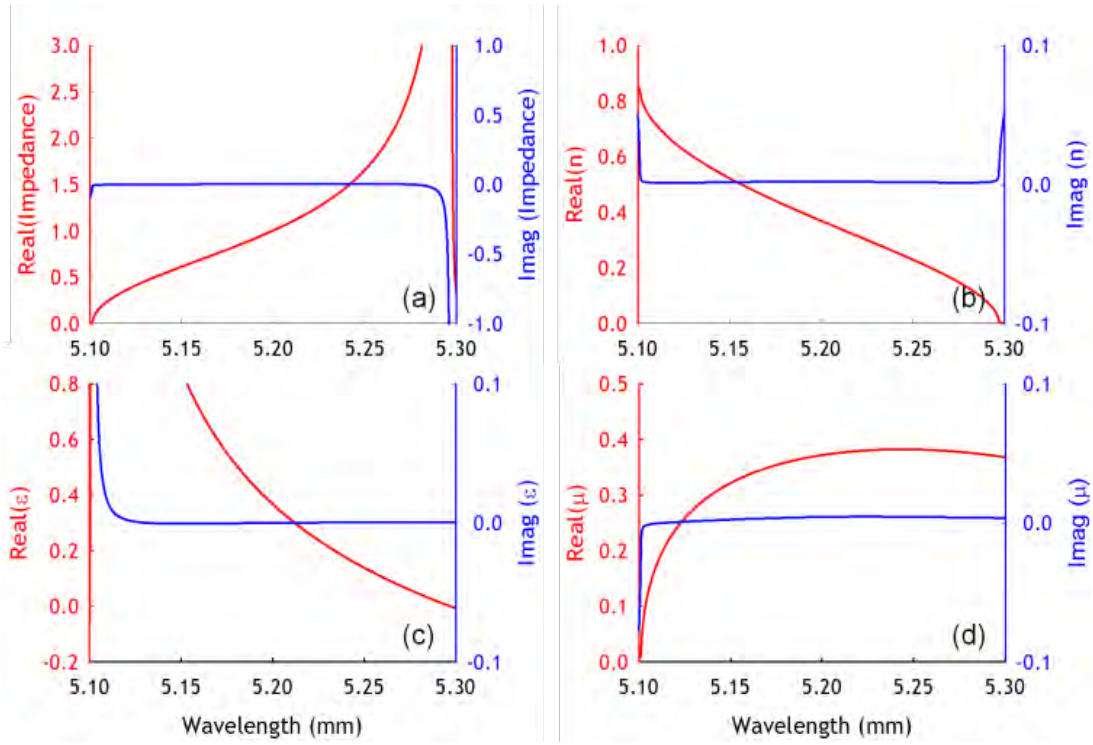

Fig. 15. Retrieved constitutive parameters of the 2-layers EOTM under normal incidence from numerical results. Real (red curve) and imaginary (blue curve) parts of: normalized characteristic impedance (a), effective index of refraction (b), electric permittivity $\boldsymbol{\varepsilon}$ (c) and magnetic permeability $\boldsymbol{\mu}$ (d).

At λ = 5.2 mm (57.7 GHz), the calculation gives $\boldsymbol{\varepsilon} = \boldsymbol{\mu} = 0.37$ [Figs. 15(c) and 15(d)], with negligible imaginary parts.

The consequences are twofold: first, the retrieved effective index of refraction is n_z = 0. 37 with a negligible imaginary part [Fig. 15(b)]; second, the real outstanding feature is that the medium is perfectly matched with free space $\eta_{EOTM} = (\boldsymbol{\mu}/\boldsymbol{\varepsilon})^{1/2} = 1$ [see Fig. 15(a)], which is the main advantage over metamaterials where ε or μ is near zero, which exhibit large difficulties in coupling the electromagnetic wave into them. Therefore, the ETM lens is operating at 5.2 mm as a near-zero metamaterial (NZM) with small ohmic losses (small imaginary part) and is matched to free space. As an additional argument, it is well known that a uniform current leads to the radiation pattern with the highest directivity, [29].

Assuming an ideal uniform current sheet source along x with the same dimensions as the central part of our lens (composed of two stacked layers) (i.e., 9 holes x d_x = 27 mm), the beamwidth between first nulls computed analytically leads to a value of 22.4°, similar to the measured values for the ETM lens reported here: 21.4°. This suggests a true NZM performance since a perfect NZM would generate a uniform current at the output face.

The strongly selective behavior around the working frequency is also remarkable. At λ = 5.24 mm a maximum is observed in the experiment,

whereas near this maximum a relative minimum appears at λ = 5.18 mm. This aspect is discussed in the following text.

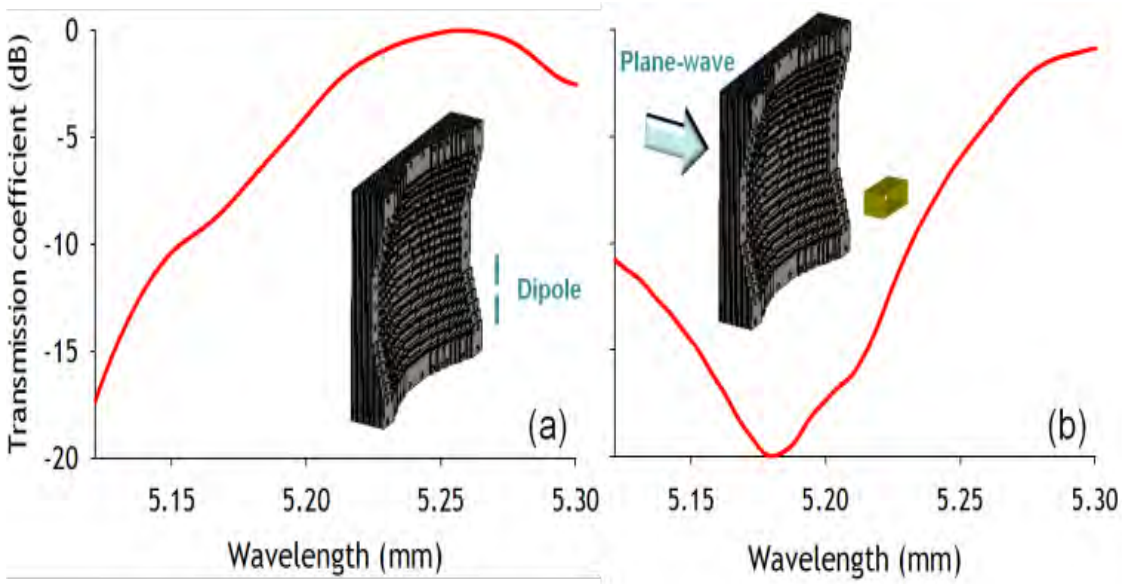

Fig. 16. Simulated normalized transmitted power in logarithm scale when the 3D EOTM-lens is illuminated by: (a) a dipole at the focal length and the field is recorded by a far-field probe at 1900 mm, and (b) a plane-wave from its flat face and the receiving antenna located at the focal length is an open-ended waveguide.

In the preceding analysis, we supported our experimental results by simplifying the problem to two stacked layers and geometrical optics (Snell's law). However, the electromagnetic response of the ETM lens is more complex since we are illuminating it in the near field: the focal length is 45 mm (8.6λ), whereas the far-field distance is $z_{ff} = 2D^2/\lambda \approx 5960$ mm, where D is the diameter of the aperture, [29]. To get a better approximation to the problem, the structure is now numerically analyzed with the time-domain solver of CST Microwave Studio, [43].

To gain more insight, we simulated the three-dimensional (3D) structure excited by a dipole at the focal length and recorded the field at 1900 mm (optical axis) with a farfieldprobe. In addition, the inverse problem was simulated (excitation by a plane wave from the flat face and detection by an open-ended waveguide at the focal length) so as to evaluate the importance of the receiver/feeder. Figure 16 shows the normalized transmission coefficient as a function of frequency for both scenarios. It is significant that both cases give rise to a sudden decrease of the transmitted power in a narrow band (15 dB within a 0.13 mm span and 20 dB within a 0.12 mm span for each case), which is in qualitatively good agreement
with the measured response.

An explanation can be found in the anisotropy of the structure. In the H plane the incident polarization is TE (or S polarization), and it has been demonstrated that in this case the numerical aperture is relatively high, [39], and therefore that the field distribution should be similar for two close wavelengths. However, the story is fairly singular for the E plane. In this case, the TM(or P) polarization is relevant, and as discussed in Refs. 39 and 40 , ETM displays an

extremely narrow numerical aperture. This means that in this E plane, we may have high frequency selectivity, which allows for a good transmission level at a particular wavelength like 5.24 mm but a relatively low level at any other wavelength close to it such as 5.2 mm, which is what occurs in the experiment.

CONCLUSIONS

Metamaterials have demonstrated an attractive route to design and manufacture lenses with powerful electromagnetic properties as a result of their ability of independently tailoring electric permittivity ε and magnetic permeability μ, which can give rise to lenses with index of refraction $n = -1$ and perfect matching to free-space at the same time. The narrow frequency band associated with metamaterials that has been pointed out as one of their main drawbacks could be in turn an advantage for beamforming, since frequencies outside the design range are automatically filtered and not enhanced, thus improving the signal-to-noise level in the desired frequency range. Nevertheless, their manufacture in THz and visible spectrum is far from being trivial.

We take a step in this race towards high frequencies and carry out a deep study of bi- and plano-concave lenses made of stacked subwavelength holes arrays perforated in metallic plates (Extraordinary Transmission Metamaterial according to our notation, although also known as stacked fishnet structures) in the millimeter-wave range. We show that a simple design based on dispersion diagram and ray tracing provides an easy and correct method for rather accurate results. Besides, an optimization of the hole diameter or longitudinal lattice constant to achieve not only $n = -1$, but also free space matching could be developed. Transversal dimensions of the foci of the order of l when the lens is used for focusing have been proven. Moreover, power enhancement up to 24 dB with cross-polarization below -30 dB with regards to co-polar, when the lens is applied as antenna radiation beamforming has been measured. Since ET was first reported in optics, we are inclined to believe that LHET-lenses can find application in terahertz and optical wavelengths in hazardous environments.

This work has plenty of places for further improvements (source, single period, parametrical study of hole size and longitudinal periodicity so as to achieve free-space matching, dielectric embedding to miniaturize, etc.) so as to make this technology competitive with current state of the art of waveguide lenses and Fresnel zone plate lenses. Actually, we have shown that in terms of HPWB and FSLL this technology already exceeds eggcrate topologies and, technical aspects aside, LHET-lenses are lighter than eggcrate configurations due to their plate-air gap assembly. In any case, the results presented here are very encouraging.

Simultaneously, we have demonstrated pencil-like radiation achieved by using a near-zero effective index of refraction metamaterial lens based on stacked extraordinary optical transmission layers at millimeter waves with high gain.

In addition, cross-polar values remain low, which is an important feature from the technological perspective. These results allow us to consider the ETM lens as a dual-band plane-wave-like beam-forming device. Moreover, an EBG behavior similar to that in Refs. 34 , 35, 44 , and 45 is likely to be attainable at higher frequencies (beyond the scope of this paper). Therefore, this ETM lens could become a multifrequency device. Since the phenomenon of extraordinary transmission has been reported in all ranges of the spectrum, this technology has the possibility of being extended to any wavelength.

FUTURE RESEARCH ACTIVITY

In cooperation with Prof. Nader Engheta of University of Pennsylvania at Philadelphia, USA, we have started a novel and ambitious research aiming Fourier transform demonstration with a practical e-near-zero metamaterial lens. The approach shown here founded on ε-near-zero materials has the potential to be translated into THz or even optics.

JOURNAL PUBLICATIONS

1) M. Navarro-Cía, M. Beruete, I. Campillo, and M. Sorolla, “Enhanced lens by near-zero metamaterial boosted by extraordinary optical transmission,” Physical Review B, 83, 115112 (2011).

2) M. Navarro-Cía, M. Beruete, I. Campillo, and M. Sorolla, “Beamforming by Left-Handed Extraordinary Transmission Metamaterial bi- and plano-concave lens at millimeter-waves,” IEEE Transactions on Antennas and Propagation, Vol 59, No. 6, pp. 2141-2151, June 2011.

CONFERENCE PUBLICATIONS

1) M. Navarro-Cía, M. Beruete, and M. Sorolla, Stacked Cut-off Hole Arrays for Lens Antennas at Subterahertz Frequencies, 5th European Conference on Antennas and Propagation 2011, EuCAP2011, Rome, Italy, April (2011).

2) M. Navarro-Cía, M. Beruete, F. Falcone, and M. Sorolla, Novel antennas based upon extraordinary transmission metamaterial lenses, INVITED in SPIE Defense, Security, and Sensing 2011, Radar Sensor Technology XV, Orlando, U.S.A., April (2011).

3) M. Navarro-Cía, V. Torres, F. Falcone, M. Beruete, and M. Sorolla, Extraordinary Transmission Lenses: different paths towards focusing enhancement, IEEE AP-S International Symposium on Antennas and Propagation 2011 and USNC/URSI National Radio Science Meeting 2011 (2011 IEEE AP-S/URSI), Spokane, U.S.A., July (2011).

4) M. Navarro-Cía, M. Beruete, M. Sorolla, and N. Engheta, Lens Concept Using Epsilon Near-Zero (ENZ) Metamaterials, INVITED in IEEE AP-S International Symposium on Antennas and Propagation 2011 and USNC/URSI National Radio Science Meeting 2011 (2011 IEEE AP-S/URSI), Spokane, U.S.A., July (2011).

5) M. Navarro-Cia, M. Beruete, V. Torres, F. Falcone, M. Sorolla, and N. Engheta, Epsilon-Near-Zero Metamaterials for Millimetre-Waves Lenses, 33rd ESA Antenna Workshop on Challenges for Space Antenna Systems, ESTEC, Noordwijk, The Netherlands, October (2011).

6) M. Navarro-Cia, M. Beruete, V. Torres, F. Falcone, and M. Sorolla, Revival of Metallic Lenses By Extraordinary Transmission Metamaterials, 33rd ESA Antenna Workshop on Challenges for Space Antenna Systems, ESTEC, Noordwijk, The Netherlands, October (2011).

REFERENCES

[1] W. Rotman, “Plasma simulation by artificial dielectrics and parallel-plate media,” *IEEE Trans. Antennas Propag.*, vol. 10, no.1, pp. 82-95, January 1962.

[2] W. E. Kock, “Metal-lens antennas,” *Proc. IRE*, vol. 34, no. 11, pp. 828–836, 1946.

[3] W. E. Kock, “Path-Length Microwave Lenses,” *Proc. IRE*, vol. 37, no. 8, pp. 852–855, 1949.

[4] A. R. Dion, and L. J. Ricardi, “A variable-coverage satellite antenna system,” *Proc. IRE*, vol. 59, no.2, pp. 252-262, 1971.

[5] J.B. Pendry, A.J. Holden, D.J. Robbins and W.J. Stewart, “Magnetism from conductors and enhanced nonlinear phenomena,” *IEEE Trans. Microw. Theory Tech.*, vol. 47, no. 11, pp. 2075-2084, 1999.

[6] V.G. Veselago, “The electrodynamics of substances with simultaneously negative values of e and m,” *Sov. Phys. Usp.*, vol. 10, no. 4, pp. 509-514, 1968.

[7] L. Solymar, and E. Shamonina, *Waves in Metamaterials*, New York: Oxford University Press, 2009.

[8] J.B. Pendry, “Negative refraction makes a perfect lens,” *Phys. Rev. Lett.*, vol. 85, no. 18, pp. 3966–3969, 2000.

[9] S.A. Ramakrishna, J.B. Pendry, D. Schurig, D.R. Smith and S. Schultz, “The asymmetric lossy near-perfect lens,” *J. Mod. Opt.*, vol. 49, no. 10, pp. 1747-1762, 2002.

[10] S. Zhang, W. Fan, N.C. Panoiu, K.J. Malloy, R.M. Osgood, and S.R.J. Brueck, “Experimental Demonstration of Near-Infrared Negative-Index Metamaterials,” *Phys. Rev. Lett.*, vol. 95, no. 13, pp. 137404-1-4, 2005.

[11] G. Dolling, C. Enkrich, M. Wegener, C.M. Soukoulis and S. Linden, “Simultaneous Negative Phase and Group Velocity of Light in a Metamaterial,” *Science*, vol. 32, no. 5775, pp. 892-894, 2006.

[12] M. Beruete, M. Sorolla, and I. Campillo, “Left-handed extraordinary optical transmission through a photonic crystal of subwavelength hole arrays,” *Opt. Express*, vol. 14, no. 12, pp. 5445-5455, 2006.

[13] M. Beruete, M. Sorolla, I. Campillo, J. S. Dolado, L. Martín-Moreno, J. Bravo-Abad, and F. J. García-Vidal, “Enhanced millimetre wave transmission through subwavelength hole arrays,” *Optics Letters*, vol. 29, no. 21, pp. 2500-2502, 2004.

[14] M. Beruete, M. Sorolla, I. Campillo, and J.S. Dolado, “Increase of the Transmission in Cut-Off Metallic Hole Arrays,” *IEEE Microw. Wireless Compon. Lett.*, vol. 15, no. 2, pp. 116-118, 2005.

[15] M. Navarro-Cía, M. Beruete, M. Sorolla, and I. Campillo, “Negative refraction in a prism made of stacked subwavelength hole arrays,” *Opt. Express*, vol. 16, no. 2, pp. 560-566, 2008.

[16] M. Beruete, M. Navarro-Cia, M. Sorolla, and I. Campillo, “Planoconcave lens by negative refraction of stacked subwavelength hole arrays,” *Opt. Express*, vol. 16, no. 13, pp. 9677-9683, 2008.

[17] M. Navarro-Cía, M. Beruete, M. Sorolla, and I. Campillo, "Converging Biconcave Lens owing to a Left-Handed Extraordinary Transmission Metamaterial," *Appl. Phys. Lett.*, vol. 94, no. 14, pp. 144107-1-3, 2009.

[18] C.G. Parazzolli, R.B. Greegor and M.H. Tanielian, "Development of Negative Index of Refraction Metamaterials with Split Ring Resonators and Wires for RF Lens Applications," in *Physics of Negative Refraction and Negative Index Materials* (Springer Series in Materials Science 98), Berlin Heidelberg, 2007.

[19] P. Vodo, P. V. Parimi, W. T. Lu, and S. Sridar, "Focusing by planoconcave lens using negative refraction," *Appl. Phys. Lett.*, vol. 86, no. 20, pp. 201108-1-3, 2005.

[20] B. Gralak, S. Enoch, and G. Tayeb, "Anomalous refractive properties of photonic crystals," *J. Opt. Soc. Am. A*, vol. 17, no. 6, pp. 1012-1020, 2000.

[21] S. Cornbleet, *Microwave Optics: The Optics of Microwave Antenna Design*, (Pure and Applied Physics 41), London: Academic Press, 1976, appx. 1.

[22] N. Engheta and R. W. Ziolkowski, "A Positive Future for Double-Negative Metamaterials*," IEEE Trans. Microw. Theory Tech.*, vol. 53, no.4, pp. 1535-1556, 2005.

[23] M. Beruete, I. Campillo, M. Navarro-Cía, F. Falcone, and M. Sorolla Ayza, "Molding Left- or Right-Handed Metamaterials by Stacked Cutoff Metallic Hole Arrays," *IEEE Trans. Antennas Propag.*, vol. 55, no. 6, pp. 1514-1521, 2007.

[24] M. Beruete, M. Sorolla, M. Navarro-Cía, F. Falcone, I. Campillo, and V. Lomakin, "Extraordinary transmission and left-handed propagation in miniaturized stacks of doubly periodic subwavelength hole arrays," *Opt. Express*, vol. 15, no. 3, pp. 1107-1114, 2007.

[25] M. Beruete, M. Navarro-Cía, M. Sorolla and I. Campillo, "Negative refraction through an extraordinary transmission left-handed metamaterial slab," *Phys. Rev. B*, vol. 79, no. 19, 195107-1-6, 2009.

[26] M. Beruete, M. Navarro-Cía, and M. Sorlla, "Strong lateral displacement in polarization anisotropic extraordinary transmission metamaterial," *New J. Phys.*, vol. 12, no. 6, 063037-1-15, 2010.

[27] A. Alù, M. G. Silveirinha, A. Salandrino, and N. Engheta, Phys. Rev. B 75, 155410, 2007.

[28] P.F. Goldsmith, *Quasioptical Systems - Gaussian Beam, Quasioptical Propagation, and Applications*, New York: Wiley IEEE Press, 1998.

[29] C.A Balanis, *Antenna Theory Analysis and Design*, New York: John Wiley & Sons, 1997.

[30] M. Beruete, I. Campillo, J. E. Rodríguez-Seco, E. Perea, M. Navarro-Cía, I. J. Núñez-Manrique, and M. Sorolla, "Enhanced Gain by Double-Periodic Stacked Subwavelength Hole Array," *IEEE Microw. Wireless Compon. Lett.*, vol. 17, no. 12, pp. 831-833, 2007.

[31] M. Beruete, M. Navarro-Cía, F. Falcone, M. Sorolla, I. Campillo, J.E. Rodríguez-Seco, E. Perea, I.J. Núñez-Manrique, "Extraordinary Transmission Surfaces as Superstrates," in *Proc. Mediterranean Microwaves Symposium 2009, MMS'09*, Tangier, 2009.

[32] I. V. Minin, and O. V. Minin, *Basic Principles of Fresnel Antenna Arrays*, Berlin Heidelberg: Springer Lecture Notes in Electrical Engineering 19, 2008.
[33] H. D. Hristov, *Fresnel Zones in wireless links, zone plate lenses and antennas*, Norwood, MA: Artech House Inc., 2000, ch. 5.
[34] S. Enoch, G. Tayeb, P. Sabouroux, N. Guerin, and P. Vincent, Phys. Rev. Lett. 89, 213902 (2002).
[35] A. Martinez, M. A. Piqueras, and J. Marti, Appl. Phys. Lett. 89, 131111 (2006).
[36] Chen, T. M. Grzegorczyk, B.-I. Wu, J. Pacheco Jr., and J.A. Kong, Phys. Rev. E 70, 016608 (2004).
[37] D. R. Smith, D.C. Vier, T. Koschny, and C.M. Soukoulis, Phys. Rev. E 71, 036617 (2005).
[38] S. A. Ramamrishna and T. M. Grzegorczyk, Physics and Applications of Negative Refractive Index Material (CRC Press, Boca Raton, FL, 2009).
[39] M. Beruete, M. Navarro-Cia, and M. Sorolla, New J. Phys. 12, 063037-1 (2010).
[40] M. Beruete, M. Navarro-Cia, M. Sorolla, and I. Campillo, Phys. Rev. B 79, 195107 (2009).
[41] L. Landau and E. M. Lifschitz, Electrodynamics of Continuous Media, Elsevier, New York, 1984.
[42] P. A. Belov, E. A. Yankovskaya, I. V. Melchakova, and C. R. Simovski, Opt. Spectrosc. (USSR) 109, 90 (2010)
[43] www.cst.com
[44] R. W. Ziolkowski, Phys. Rev. E 70, 046608 (2004).
[45] S. J. Franson and R. W. Ziolkowski, IEEE Antennas Wireless Propag. Lett. 8, 387 (2009).

LIST OF SYMBOLS, ABBREVIATIONS, AND ACRONYMS

º sexagesimal degree

a coordinate of the lens equation

b abscissa of the lens equation

c speed of light

D largest dimension of the antenna

D_l circular lens of diameter

Δ spatial resolution

d_z longitudinal lattice constant

d_x and d_y transversal lattice constants

ε dielectric permittivity

f frequency

f_{co} wave cut-off frequency

f distance between the focus and the lens

h hole diameter

η wave impedance

k wavenumber

λ wavelength

μ magnetic permeability

n index of refraction

θ angle of emergence of the scattered wave with respect to the normal

v_p phase velocity of the electromagnetic wave

w metal thickness

ω angular frequency

2D Two Dimensional

3D Three Dimensional

CST Computer Simulation Technology

dB decibel

deg degree

EBG Electromagnetic Band Gap

ET Extraordinary Transmission

ETM Extraordinary Transmission Metamaterial

FNBW First Null Beamwidth

FSLL First Side Lobe Level

GHz Gigahertz

HPBW Half-Power Beamwidth

LH Left-handed

LHET Left-Handed Extraordinary Transmission

LHM Left-Handed Media

m meter

mm millimeter

NIR Negative Index of Refraction

NZM Near Zero Metamaterial

PEC Perfect Electrical Conductor

S siemens

SRR Split-Ring Resonator

TE Transversal Electric Wave

TEM Transversal Electromagnetic Wave

THz Terahertz

TM Transversal Magnetic Wave